Icarus **147**, 180–204 (2000)
doi:10.1006/icar.2000.6420, available online at http://www.idealibrary.com on IDEAL®

The HB Narrowband Comet Filters: Standard Stars and Calibrations

Tony L. Farnham[1] and David G. Schleicher

Lowell Observatory, 1400 Mars Hill Road, Flagstaff, Arizona 86001

and

Michael F. A'Hearn

Department of Astronomy, University of Maryland, College Park, Maryland 20742

Received May 17, 1999; revised February 29, 2000

We present results concerning the development and calibration of a new set of narrowband comet filters, designated the HB filter set, which was designed and manufactured to replace aging IHW filters. Information is also presented about the design and manufacturing of the filters, including the reasoning that was used for deciding the final wavelengths and bandpasses. The new filters are designed to measure five different gas species (OH, NH, CN, C_2, C_3), two ions (CO^+, H_2O^+), and four continuum points. An improved understanding of extended wings from emission bands in comet spectra, gained since the development of the IHW filters, was incorporated into the new design, so that contamination from undesired species is significantly reduced compared to previous filters. In addition, advances in manufacturing techniques lead to squarer transmission profiles, higher peak transmission and UV filters with longer lifetimes.

We performed the necessary calibrations so that data obtained with the filters can be converted to absolute fluxes, allowing for, among other things, accurate subtraction of the continuum from the gas species. Flux standards and solar analogs were selected and observed, and the data were used to establish a magnitude system for the HB filters. The star measurements were also used to evaluate which solar analogs were best representatives of the Sun and to explore how the flux standards differed in the UV with respect to their spectral type. New procedures were developed to account for the non-linear extinction in the OH filter, so that proper extrapolations to zero airmass can be performed, and a new formalism, which can account for mutual contaminations in two (or more) filters, was developed for reducing comet observations. The relevant equations and reduction coefficients are given, along with detailed instructions on how to apply them. We also performed a series of tests involving factors that can affect either the filter transmission profiles or the distribution of the emission lines in the gas species to determine how these effects propagate through to the calibration coefficients. The results indicate that there are only two factors that are a concern at a level of more than a few percent: f-ratios smaller than $f/4$, and a few individual filters whose transmission profiles are significantly different from the filters used in the calibrations. © 2000 Academic Press

Key Words: **comets; comets, composition; comets, Hale–Bopp; photometry; data reduction techniques.**

1. INTRODUCTION

Comets are widely regarded as the least processed remnants from the formation of the Solar System which are currently accessible for detailed study. As such, compositional investigations are especially important in providing clues to the relative abundances within the proto-solar nebula in general and to the temperatures in the outer Solar System where comets are believed to have coalesced. While *in situ* measurements are clearly preferred and will become more common in the coming decades, the comae of only three comets have been directly sampled thus far. Similarly, rapid improvements in infrared and radio instrumentation now permit the study of parent molecules which directly originate from the nucleus, rather than the daughter species which are primarily observable in the near-ultraviolet and visible regions of the spectrum. However, more comets are accessible in the visible than any other spectral region, and measurements in this regime continue to play a critical role in compositional investigations.

Narrowband interference filters, specifically designed to isolate continuum points and some of the stronger emission bands in cometary spectra, have now been in use for over 25 years (cf. A'Hearn and Cowan 1975). Appropriate calibration of photometric measurements permits the determination of continuum-subtracted emission band fluxes which, with appropriate modeling, can yield column densities, total abundances, and production rates of the species in question. The continuum measurements also provide fluxes which, again with modeling, can yield dust production rates and constrain physical properties of the dust particles. Photometry and imaging with narrowband filters have both advantages and disadvantages when compared to

[1] Present address: Department of Astronomy, University of Texas, Austin, TX 78712. Fax: (512) 471-6016, E-mail: farnham@astro.as.utexas.edu.

0019-1035/00 $35.00
Copyright © 2000 by Academic Press
All rights of reproduction in any form reserved.

spectrophotometry. For example, aperture photometry can measure larger fractions of the total coma than can be obtained in the slit of a spectrograph, and CCD imaging can be used for morphological studies of individual species such as in the discovery of CN jets in Comet 1P/Halley (A'Hearn *et al.* 1986). The larger fields of view also provide better contrast of the gas to underlying continuum, since most gas species fall off in intensity less steeply than the dust. Furthermore, small telescopes, which are often more readily available, can be efficiently used with these techniques. Disadvantages of the narrowband filters are that weak emission features, such as those from CH and NH_2, are impractical to isolate, and measurements of relative line intensities and bandshapes require spectroscopy. Finally, weak emission features are located throughout most of the visible spectrum, so contamination of continuum measurements is a significant issue that must be addressed when designing and using filters.

Early implementations of narrowband comet filters (e.g., O'Dell and Osterbrock 1962) produced mixed results, with major discrepancies in the conclusions, due to the different filters being used by different observers. In the past quarter century, however, several generations of narrowband comet filters have been employed by an increasing number of observers. The first version consisted of a single set of five filters that isolated CN, C_2, C_3, and continuum and was used by A'Hearn and Cowan (1975) and A'Hearn *et al.* (1977) for Comets Kohoutek (1973 XII) and West (1976 VI), respectively. The first standardized filters consisted of three sets of up to 10 filters, which were used from 1976 to 1983. This set initially included the three carbon species and associated continuum points, with the OH, NH, and UV continuum filters added in late 1979 (cf. A'Hearn *et al.* 1979, A'Hearn and Millis 1980). In 1984, these sets were replaced by the International Halley Watch (IHW) standardized filters, which were based on design recommendations of an IAU Commission 15 Working Group. In addition to several dozen sets of nine 1-inch filters—OH, CN, C_2, C_3, CO^+, H_2O^+, and three continuum points—for photoelectric photometers, about 15 38-mm image-quality sets were produced for CCD imaging (cf. Osborn *et al.* 1990, A'Hearn 1991, Larson *et al.* 1991). In the intervening years, the use of these standardized filters by observers around the world has greatly facilitated the intercomparison of data sets of a myriad of comets in addition to Comet Halley. Unfortunately, interference filters tend to physically degrade with time, often with significant decreases in peak transmission and shifts in wavelength. These problems are especially true for near-UV filters due to manufacturing techniques, and many, if not most, of the IHW filter sets have suffered from these effects.

While the need for replacement filters for the IHW sets has been evident for several years (cf. Schleicher *et al.* 1991), it was the discoveries of Comets Hale–Bopp (1995 O1) and Hyakutake (1996 B2) that provided the impetus for NASA to fund the design and manufacture of new filters, along with the establishment of a standard star system and the determination of all of the necessary reduction coefficients for the filters. In the spring of 1996 we agreed to perform these tasks, and filter design and bidding took place during the summer. The order was placed with the selected manufacturer, Barr Associates, Inc., in September 1996, and all filters were received and re-distributed to observers by February 1997. Observations to establish the standard star magnitude system were completed in April 1998 and the filter calibration procedures were developed and executed throughout 1998. In early 1999, a technique was finalized for reproducing the non-linear extinction in the OH filter. Although much of this effort could have been avoided by using the same filter specifications as for the IHW sets, a significantly better filter set could be produced by starting from scratch, because of improvements in our understanding of the large degree of contamination of the IHW continuum filters and in manufacturing techniques for near-UV filters. The resulting 11 filters have bandpasses that are squarer and, in many cases, have higher throughput than previous sets, and the continuum filters are all located in spectral regions with less contamination. Also, the near-UV filters are expected to have a significantly longer useful lifetime, and it is reasonable to expect that these filters will still be in use 15 or 20 years in the future.

Because the first, and most extensive, use of the new filters was with Comet Hale–Bopp, we have designated them the HB filter set. Overall, a total of 48 full or partial sets were produced, including 14 sets for users outside of the United States; the majority of the latter were purchased with funds separate from the NASA grant. Reflecting the changing instrumentation at most observatories, the majority of the recipients requested larger-format filters for use with CCDs, in contrast to the IHW sets where two-thirds of the filters were only 1-in. in size, for use with photoelectric photometers.

To maximize the results obtainable with these filters, recipients must be able to calibrate their data in an absolute manner, and the procedures and parameters for doing this are the primary subject of this paper. Note that in support of the Rosetta spacecraft mission scheduled for launch in 2003, a near-concurrent effort to produce new filters was undertaken by ESA in order to observer the Rosetta target, Comet 46P/Wirtanen, during its 1996/97 apparition. Unfortunately, these unavoidably independent efforts resulted in somewhat different design preferences and specifications between our HB sets and the ESA-sponsored filters.

In the following sections, we will discuss the detailed specifications of the HB filters and how they differ from their predecessors, the new set of flux standards and the resulting standard star magnitudes, and the solar analogs that are used to establish the shape of the solar spectrum for continuum subtraction from the emission band measurements and to provide a measure of the color of the underlying dust. We also describe our improved methodology for removing contamination by unwanted emissions and provide the relevant coefficients for reducing observations to absolute fluxes. In addition, we address the problems produced by non-linear extinction in the OH filter and introduce a more sophisticated technique for modeling the

curvature than was used in the IHW filter reductions. Along the way, we present results regarding the near-UV observations of the flux standards and solar analogs, which showed unexpected diversity. These results directly impact the search for a true solar "twin" in studies of solar evolution, in addition to the practical aspect of establishing which stars best-match the solar spectrum so they can be used in numerous Solar System studies. Finally, Appendix A describes the procedures used for computing the OH extinction. Appendices B and C contain details about how the standard star magnitudes and absolute fluxes were determined, and Appendix D lists the equations and basic procedures needed for fully reducing observations obtained with the HB filters.

2. DESIGN AND MANUFACTURING OF THE HB FILTER SET

The design process of a new filter set is necessarily a series of compromises between numerous competing issues. This was particularly true for the HB filters. In the case of an emission band, for instance, a wider filter can increase the fraction of the total band that is measured, but at the expense of even greater continuum flux and, therefore, lower contrast of emission to continuum. Wider continuum filters yield higher signal-to-noise, but often with increased contamination by weak emission features—a negligible effect for a comet as dusty as Hale–Bopp, but quite important for high gas-to-dust comets such as Encke, where the IHW UV continuum filter is dominated by C_3 contamination. Manufacturing constraints for the narrowband interference filters were another design consideration. The most important of these were the nominal tolerances, amounting to 10% of the FWHM, in both the center wavelength and the FWHM. The wavelength shift induced by differing telescope f-ratios provided yet another constraint; all of the filters were designed to accommodate f-ratios as small as $f/4$ without requiring adjustments to the calibration procedures. Finally, the minimum viable bandwidth for any filter was approximately 40 Å for a variety of reasons, including low flux levels in faint comets, unacceptably large wavelength shifts for low f-ratio systems, and the degree of uniformity obtainable among manufacturing batches. Incorporating all of these constraints into the design resulted in final specifications which were slightly offset redward to accommodate small f-ratios, generally wider for emission band filters than otherwise would be required to ensure the entire band would be transmitted and narrower for continuum bands to prevent encroachments by nearby emission features.

The decision as to which cometary emission bands and continuum regions to isolate with narrowband filters was based on three primary factors: considerable experience working with both the IHW filter set and the earlier filter set by A'Hearn and Millis (1980), discussions with several other experienced users of the IHW filters, and examination of numerous spectra obtained both in our own studies and those supplied by A. Cochran and H. Spinrad, particularly of high gas-to-dust comets such as Encke and deVico. Ultimately, the same specific emission bands of the same species—OH, NH, CN, C_3, C_2, CO^+, and H_2O^+—were selected for inclusion as were chosen for the IHW filter set. (In fact, NH was not offically included in the IHW set but, rather, an NH filter from the earlier A'Hearn and Millis sets was used to supplement the IHW set in our own studies.) Other species, such as NH_2 and CH, were excluded due to the difficulty in obtaining accurate continuum subtraction for the relatively weak emission features of these short-lived molecules. As will be discussed in detail later, all of the HB continuum filters are located at different wavelengths from the IHW filters because of additional knowledge gained since the design of the IHW set.

We now present some pertinent issues regarding the emission bands and how they are used to constrain the filter specifications. The filters can be naturally grouped based on the characteristics of the emission band shapes and whether or not the shape can change significantly. The neutral, heteronuclear species—OH, NH, and CN—all produce relatively narrow bands whose line intensities vary as a complex function of heliocentric velocity and/or distance, due to the Swings effect (Swings 1941). Fortunately, theoretical fluorescence calculations of the line intensities for each of these species have been produced by multiple researchers. Comprehensive sets of synthetic spectra, which were available and were used in our analysis, include OH by Schleicher and A'Hearn (1988), NH by Kim *et al.* (1989) and Meier *et al.* (1998), and CN by Schleicher (1983). Using these computed spectra allowed us to consider the changing bandshapes when determining the exact placement of the bandpasses. In the case of OH, the filter isolates the 0-0 band at 3090 Å, while excluding the 1-1 band which starts at 3126 Å. For NH, while the 1-1 band overlaps the 0-0 band, virtually the entire signal is produced by the 0-0 band, due to the extreme, diagonal nature of the Franck–Condon parabola. The CN filter includes both the 0-0 band and the overlapping 1-1 band, the latter varying between 5 and 11% of the flux of the 0-0 band due to the Swings effect. To ensure that the high rotation level lines (which are populated when a comet is at small heliocentric distances) are included in the bandpass, the CN filter is wider at the blue end than the IHW filter. It is also unavoidably contaminated by the blue wing of the C_3 band. For the OH, NH, and CN filters, our objective was to include the entire band(s) within the nearly flat-topped portion of the bandpass, so that redistribution of the emission line strengths within the band by the Swings effect will not affect the calibrations; this objective was essentially reached (see the filter calibration section for further details).

The homonuclear molecules, C_2 and C_3, have relatively broad emission bands because large numbers of rotational levels are populated in each vibrational level and multiple vibrational bands overlap in wavelength with comparable band intensities. Moreover, because C_3 is a triatomic homonuclear molecule, this effect is exaggerated further, resulting in a single band complex whose wings stretch from approximately 3400 to 4400 Å. In neither species is it practical to measure an entire band, and so the filter bandpass, in each case, has been designed to measure a specific portion of the band(s) including the band peaks. However,

only two of the four primary C_3 peaks are included, because the short wavelength cutoff of the C_3 filter was chosen to avoid the CO^+ (3-0) band near 4000 Å. The C_2 filter is slightly wider at the blue end than the IHW filter, to minimize the effect of small variations in the bandpass between manufacturing batches. A weak NH_2 band unavoidably contaminates the C_2 filter.

Both ions, CO^+ and H_2O^+, have several well-defined bands. The CO^+ 2-0 band at 4260 Å was selected for the HB filter, because the stronger band at 4010 Å overlaps peaks in the C_3 band complex, while other bands either are weaker or have more contamination than the 4260-Å band. The CO^+ filter avoids the CN ($\Delta v = -1$) band at the blue end and CH emission at the red end, but is contaminated by the long redward wing of C_3. The other ion filter, H_2O^+, was designed to isolate the (0, 6, 0) band centered near 7010 Å. Although narrower than the IHW filter, H_2O^+ is the widest of the HB filters and includes the entire band within its flat top. It was decided that, in most circumstances, it was preferable to maximize the H_2O^+ flux at the expense of greater continuum flux, because the ion tail is often separate from the dust tail, allowing ion morphology to be distinguished from dust features. An NH_2 band contaminates this filter; however, all other H_2O^+ bands are weaker and/or are contaminated by species having longer lifetimes.

The just-described decisions involved in the placement of the HB emission band filters resulted in essentially the same bandpasses as were selected for the IHW set, with only small changes in locations and widths of filters. In contrast, the choice of bandpasses for isolating the continuum differed considerably from the IHW specifications, which were recommended by the IAU Commission 15 Working Group. Shortly after the IHW calibration was completed, it became apparent that the C_2 contamination of the 4845-Å filter was more severe than originally believed and that the degree of contamination varied with distance from the nucleus for a given gas-to-dust ratio. It was also determined that the UV continuum filter at 3645 Å was substantially contaminated by the very long blue wing of the C_3 band, which is often not evident in comet spectra due to the shape of the solar continuum reflected from the dust. In previous filter sets, this contamination produced an artificially elevated UV continuum, yielding blue "continuum" colors in comets with low dust-to-gas ratios and negative fluxes for CO^+ after continuum subtraction. Finally, an emission feature sometimes attributed to NH_2 is located within the IHW red continuum filter at 6840 Å. When designing the new filters, we used this increased knowledge of contaminants to improve the placement of the continuum measurements. First, the UV filter was moved shortward to 3448 Å, which reduces the C_3 contamination, places the filter closer to the OH and NH bands, and increases the overall continuum baseline for color measurements. While this new HB filter (designated UC) is contaminated by weak OH and CO_2^+ emission (Valk *et al.* 1992), C_3 remains the primary contaminant, although at a much lower level than for the IHW filter. Next, the mid-continuum point (designated GC, for green continuum) was moved to the other side of the C_2 ($\Delta v = 0$) band, and placed at 5260 Å, a location which has reduced C_2 contamination, avoids most NH_2 emission, and is similar to the earlier A'Hearn and Millis (1980) continuum point. The red continuum (RC) filter was also moved longward, to the other side of the H_2O^+ band, to avoid a recurring emission band known to exist in the IHW filter and to again increase the continuum baseline. This filter, at 7128 Å, has low transmission cut-offs (10%) at 7097 and 7169 Å to avoid the H_2O^+ emission at the blue end and a telluric H_2O feature at the red end. Finally, a new continuum filter was added at 4450 Å, a relatively clean location near the CO^+ and C_2 bands. It avoids C_2 emission on either side, but two pairs of very weak, apparently unidentified, recurring features are within the bandpass. This new blue filter (BC), combined with the GC filter, permits continuum subtraction for the CN, C_3, CO^+, and C_2 filters without needing UV continuum measurements, which are difficult to obtain at low elevation sites or with CCDs that have poor UV-sensitivity.

Besides the locations of the continuum filters, the most significant change from the IHW filters to the HB filters was the improved shape and peak of the transmission profiles due to advances in manufacturing techniques. The improvements in basic bandpass characteristics were greatest below 4000 Å, where the IHW filters were near-Gaussian in shape with peak transmissions of only 30–40%. Except for the red continuum filter (where a four-cavity design was used), five-cavity designs were utilized for each HB filter, resulting in near-square filter transmission profiles (see Table I and Fig. 1). Typical peak transmissions ranged from 56% in the near-UV to 85% in the visible and near-IR, and all filters are blocked to minimize red leaks. The OH filter has a small red leak (~0.03%) at 3350 Å, but all other filters are good to a level better than 10^{-5}. All filters are image-quality, have hard, anti-reflection coatings, and were designed to be par-focal. Finally, with the new manufacturing techniques, the expected lifetime of the near-UV filters is anticipated to match that of the visible wavelength filters.

As stated earlier, 48 full or partial filter sets were produced, with sizes ranging from 1-in. round to 4-in. square. The filters were produced in batches between December 1996 and February 1997, and although all batches of a particular filter were manufactured to the same specifications, there are small differences from filter to filter due to variations within an evaporation run and to differences between runs. As batches were finished, the filters were shipped from the manufacturer to Lowell Observatory, where like filters were compared and then distributed to individual observers. For the purposes of determining the filter calibrations, we selected a filter at each wavelength whose characteristics best represented all of the filters for that bandpass. The measured characteristics (central wavelength, bandwidth, transmission, etc.) of this representative filter set are listed in Table I. Typically, more than half of the filters have transmission profiles essentially identical to their representative filter, with the rest of the group having small wavelength shifts or slight differences in the shape of the transmission profile. Unfortunately, there are a few C_2 and C_3 filters (mostly large format imaging filters)

TABLE I
Representative Filter Characteristics

Species	ID	Designation	Transmission[a] (%)	CW[b] (Å)	Power point width[c] (Å) 80%	50%	10%	1%
OH (0-0)	OH	3090/62	56	3097	52	58	68	87
NH (0-0)	NH	3362/58	63	3361	47	54	64	81
UV continuum	UC	3448/84	67	3449	72	79	93	116
CN (Δv=0)	CN	3870/62	67	3869	50	56	65	82
C_3 (Swings system)	C3	4062/62	62	4063	43	58	69	84
CO^+ (2-0)	CO+	4266/64	77	4266	58	64	74	90
Blue continuum	BC	4450/67	65	4453	55	61	71	86
C_2 (Δv=0)	C2	5141/118	85	5135	109	119	140	171
Green continuum	GC	5260/56	78	5259	52	56	65	79
H_2O^+ (0,6,0)	H2O+	7020/170	75	7028	148	164	193	239
Red continuum	RC	7128/58	80	7133	53	58	71	92

[a] Measured mean peak transmission.
[b] Measured center wavelength.
[c] Measured full-width power points.

whose transmission profiles are shifted by up to 10 Å from our representative filter, and for the worst of these cases, the calibration coefficients discussed later may be off by as much as 10%. A further complication is that the transmission profile may vary slightly across the surface of the large-format imaging filters. However, it should be emphasized that these problems are less severe than they were for any of the previous filter sets. Other issues that should be recognized in the HB filters include the problems associated with usage under non-optimum conditions, such as small f-ratios (which are especially a concern because many CCD cameras are operated on faster telescope systems). Details concerning these issues will be discussed in Section 5.

3. STANDARD STAR SELECTION

The design and implementation of a new set of comet filters requires the establishment of a standard star system as well as the development of standard procedures, equations, and coefficients that are used to convert data to absolute fluxes. As with the IHW filters (cf. Osborn *et al.* 1990), two types of standard stars are used in the HB calibration procedures. The first—solar analogs—represent the solar spectrum in determining the spectral reflectivity of the dust and are used for basic continuum subtraction from the comet emission bands. The relevant information from these stars is incorporated into the coefficients described below; so, in a typical comet observing program, it is not necessary to observe the solar analogs. The second type of standard star is the flux standard, which is used to determine atmospheric extinction and to convert relative magnitudes to absolute fluxes.

3.1. Solar Analogs

In early 1997, we began to select candidates for our solar analogs. Unfortunately, no single star has been found that exhibits all of the same characteristics of the Sun, so a set of stars whose collective properties approximate those of the Sun must be used. We made a major effort to choose the best solar analogs available, but will not discuss all of the details of our search here. Fortunately, during the time that we were considering our list of candidates, a solar analogs workshop was held at Lowell Observatory (Hall 1997), and we took advantage of the gathering of experts to refine the selection of stars. The first step in our selection was to define a set of criteria to identify stars that are similar to the Sun. Because the relevant information from the solar analogs is incorporated into the calibration and reduction process, it should not be necessary to observe these stars in conjunction with observations of comets; therefore, sky coverage is not an issue. The important factor here is that a solar analog should mimic the Sun as closely as possible. We require stars whose photometric colors best represent the Sun, and, for our purposes, other properties such as age are secondary. Specific criteria were identified as a means of searching for stars that represent the Sun as closely as possible in all respects: these criteria include spectral type, effective temperature (T_{eff}), B–V color, bolometric magnitude, metallicity ([Fe/H]), and to a lesser extent surface gravity (log g) and chromospheric activity. We required that all of the characteristics for each candidate be near that of the Sun, and in making our final selections, we attempted to bracket the Sun in a balanced manner for each of the different properties. A list of 12 solar analog candidates is given in Table II, with their coordinates, V magnitude, spectral type,

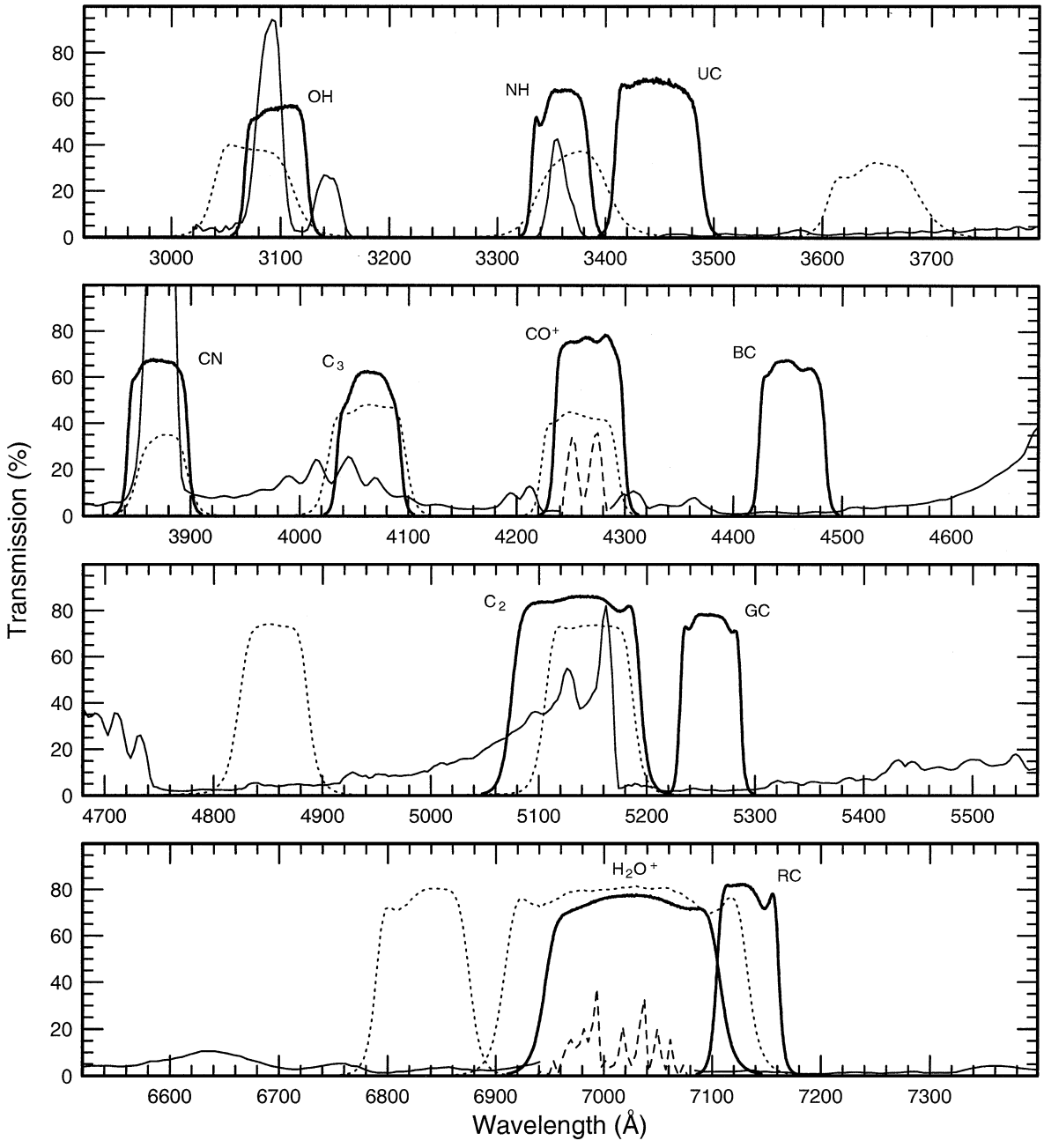

FIG. 1. Transmission profiles for the HB filters (thick lines) and for the IHW filters (dotted lines). For comparison, measured comet spectra illustrate the locations of the different emission bands. The neutral species and continuum regions are depicted by a spectrum of Comet 122P/deVico (spectral resolution = 12 Å) in the three top panels and a spectrum of Comet 8P/Tuttle (resolution ~40 Å) in the bottom panel (thin solid lines). Because these comets do not exhibit clear ion bands, the 2-0 band of CO^+ from Comet 29P/Schwassmann–Wachmann 1 (resolution = 12 Å) has been inserted from 4240–4265 Å in the second panel and the 0-6-0 band of H_2O^+ from Comet Kohoutek 1973 E1 (resolution = 5 Å) has been inserted from 6940–7080 Å in the bottom panel (dashed lines). The 122P/deVico spectrum is courtesy of A. Cochran, and the 8P/Tuttle spectrum, created by S. Larson and J. Johnson, is courtesy of S. Larson. The CO^+ band was extracted from Cochran and Cochran (1991) and Cochran *et al.* (1991) and the H_2O^+ band was extracted from Wehinger *et al.* (1974) and Wyckoff and Wehinger (1976).

and Johnson B–V and Strömgren u–b colors. The characteristics (from Cayrel deStrobel 1996, Hall 1997 and references therein) that were used as selection criteria are given in Table III, which include, for comparison, the corresponding values adopted for the Sun (several of which are not accurately known). The characteristics of these 12 stars are grouped tightly around the Sun (relative to other possible candidates), as shown in Figs. 5, 11, 12, and 14 of Cayrel deStrobel, yet they also adequately cover the range of possible values for the Sun.

After observing the candidate solar analogs with the HB filters (discussed in detail below), the data were used to re-evaluate each star to determine if it should be included in the final subset

TABLE II
Standard Star Specifications

Object[a]	Other Name	RA (J2000)	Dec	V	B–V	u–b	Spectral Type	Notes[b]
Flux Standards		h m s	° ′ ″					
HD 3379 *	53 Psc	00 36 47.24	+15 13 54.5	5.89	−0.15	+0.342	B2.5IV	1
HD 6815		01 08 55.72	+09 43 49.4	7.30	−0.06	+1.148	B9	
HD 14951		02 24 48.92	+10 36 38.9	5.46	−0.09	+0.614	B7IV	
HD 19712		03 10 18.03	−01 41 40.7	7.35	−0.03	+1.203	B9	
HD 26912 *	μ Tau	04 15 31.93	+08 53 33.5	4.27	−0.04	+0.560	B3IV	
HD 31331		04 54 50.63	+00 28 02.6	5.99	−0.12	+0.558	B5V	
HD 37112		05 36 03.50	−00 46 48.6	8.02	−0.08	+0.637	B6V	3
HD 52266 *		07 00 21.05	−05 49 36.7	7.23	−0.01	+0.063	O9V	
HD 68099		08 11 16.56	+09 49 16.9	6.07	−0.10	+0.750	B6III	
HD 72526		08 33 25.29	−00 18 29.1	7.93	+0.10	+1.371	B8	
HD 74280 *	η Hya	08 43 13.48	+03 23 55.2	4.30	−0.20	+0.248	B3V	1
HD 89688 *	23 Sex	10 21 01.97	+02 17 23.1	6.68	−0.12	+0.393	B3IV	1,4
HD 97991		11 16 11.55	−03 28 19.6	7.41	−0.22	−0.009	B1V	5
HD 120086 *		13 47 19.13	−02 26 36.8	7.90	−0.17	+0.162	B2V	1
HD 129956		14 45 30.26	+00 43 02.8	5.70	−0.04	+1.269	B9.5V	
HD 149363 *		16 34 28.22	−06 08 09.4	7.80	+0.02	+0.135	B0.5III	
HD 154445		17 05 32.14	−00 53 31.6	5.64	+0.16	+0.409	B1V	
HD 164852 *	96 Her	18 02 22.98	+20 50 01.3	5.27	−0.08	+0.436	B3IV	
HD 170783		18 31 04.35	+04 37 37.4	7.73	+0.19	+0.999	B5	
HD 187350		19 49 33.40	−01 06 03.1	8.14	+0.11	+0.270	B1V	2
HD 191263 *		20 08 38.16	+10 43 32.5	6.33	−0.14	+0.389	B3V	
HD 205130		21 33 35.23	−09 39 38.1	7.88	+0.02	+0.905	B9	6
HD 209008		22 00 07.78	+06 43 02.1	6.00	−0.12	+0.500	B3III	
HD 219188 *		23 14 00.48	+04 59 49.6	7.05	−0.20	+0.038	B0.5III	
Solar Analogs								
HD 11131		01 49 23.35	−10 42 12.8	6.77	+0.62	+1.484	G1V	7
HD 25680 *	39 Tau	04 05 20.25	+22 00 31.8	5.90	+0.62	+1.533	G5V	8
HD 28099 *	vB 64	04 26 40.13	+16 44 48.7	8.12	+0.66	+1.619	G2V	
HD 29461 *	vB 106	04 38 57.31	+14 06 20.0	7.96	+0.67	+1.621	G5V	
HD 30246 *	vB 142	04 46 30.38	+15 28 19.1	8.33	+0.67	+1.621	G5V	
HD 76151 *		08 54 17.95	−05 26 04.5	6.01	+0.65	+1.626	G3V	
HD 81809		09 27 46.80	−06 04 16.6	5.36	+0.64	+1.540	G2V	
HD 146233	18 Sco	16 15 36.38	−08 21 45.3	5.49	+0.65	+1.577	G1V	
HD 186408 *	16 Cyg A	19 41 48.93	+50 31 30.5	5.96	+0.64	+1.605	G1.5V	9
HD 186427 *	16 Cyg B	19 41 51.96	+50 31 03.3	6.20	+0.66	+1.622	G2.5V	9
HD 191854 *		20 10 13.31	+43 56 44.6	7.42	+0.66	+1.606	G5V	
HD 217014	51 Peg	22 57 27.98	+20 46 07.3	5.47	+0.67	+1.668	G2.5V	

[a] * = IHW standard star.

[b] Notes. 1. Variable star ($\Delta m < 0.05$). 2. Emission line star. 3. Nearby bright star: 1.7 mag, 142″ E, 1518″ S. 4. Nearby star: 8.9 mag 200″ W, 220″ N. 5. Nearby bright star: 4.6 mag, 420″ E, 645″ S. 6. Nearby star: 9.2 mag, 325″ W, 156.5″ N. 7. Nearby star: 4.8 mag, F0 star, 176″ E, 62″ N. 8. Nearby star: 8.8 mag, G0 star, 1.2″ E, 173″ N. 9. Cyg A and Cyg B form a double system: Cyg B is 44″ E and 27.5″ S of Cyg A.

TABLE III
Solar Analog Characteristics

Object[a]	Other name[a]	V	B–V	u–b	Physical properties						
					Spect.	T_{eff}(K)	[Fe/H]	log g	M_{bol}	Activity	Notes[b]
HD 11131		6.77	0.62	1.484	dG1	5820	–0.09	4.37	4.71	Strong	
HD 81809	HR 3750	5.36	0.64	1.540	G2	—	—	—	—	Weak	1
HD 25680	**HR 1262**	5.90	0.62	1.533	G5	5794	–0.03	4.30	4.63	Strong	
HD 146233	**18 Sco**	5.49	0.65	1.577	G2	5789	+0.05	4.45	4.53	Weak	
HD 186408	**16 Cyg A**	5.96	0.64	1.605	G1.5	5780	+0.06	4.29	4.06	Weak	
HD 29461	**vB 106**	7.96	0.67	1.621	G5	—	—	—	—	Strong	
HD 191854		7.42	0.66	1.606	G5	—	—	—	—	Weak	2
HD 186427	**16 Cyg B**	6.20	0.66	1.622	G2.5	5765	+0.05	4.30	4.30	Weak	
HD 28099	**vB 64**	8.12	0.66	1.619	G2	5777	+0.16	4.50	4.80	Strong	
HD 30246	vB 142	8.33	0.67	1.621	G5	—	—	—	—	Strong	
HD 76151	**HR 3538**	6.01	0.65	1.626	G3	5727	+0.07	4.50	4.65	Medium	
HD 217014	51 Peg	5.47	0.67	1.668	G2.5	5755	+0.06	4.18	4.73	Weak	
Sun	Sol	—	0.64	—	G2	5777	0.00	4.44	4.75	Weak	

[a] **Bold face** indicates stars included in the determination of the adopted mean solar colors.
[b] Notes. 1. Spectroscopic binary (sep < 0.5 arcsec). G0V and G9V combine to produce appearance of a G2V star. 2. Binary star (sep < 0.4 arcsec). G4V and G8V combine to produce appearance of a G5V star.

of analogs. The solar analog magnitudes are given in Table IV, and the colors, computed relative to the blue continuum filter, are listed in Table V. The colors are also plotted in Fig. 2, normalized to HD 186427 (16 Cyg B). (This star is a somewhat arbitrary choice for the normalization; it was used primarily because it is well-established as a solar analog and lies near the center of our candidates in terms of color.) The 12 stars are very similar at wavelengths longer than 4400 Å; however, there is significant variation in the near ultraviolet, which makes this region an excellent diagnostic tool for evaluating the solar analogs. Because the CN–BC color is particularly sensitive to the differences between the stars, the curves are plotted in order of increasing CN–BC for comparison to other characteristics of the stars. Relating this color to the star's spectral type shows no clear pattern, which may not be surprising given the uncertainties in assigning spectral sub-classifications and the narrow range of star types that are considered here. Strömgren u–b, on the other hand, reflects the same trends as the CN–BC color, indicating that u–b could be very useful as a discriminator for evaluating the sensitive near-ultraviolet region in other solar analogs. The CN–BC color ranges from 0.848 to 1.132 in the extreme cases, with a more typical value of 1.058 (HD 186427). For the other filters, the ranges are less extreme, to the extent that all colors above 4200 Å have a dispersion of less than 0.05 mag. See Farnham and Schleicher (1997) for further discussion of the preliminary solar analog results.

In the final selection of our solar analogs, we used three of the best solar analogs (HD 146233, HD 186408, and HD 186427), based on the consensus of the participants at the Lowell Solar Analogs Workshop, as a starting point and eliminated stars whose colors differed drastically from these three. For the remaining stars, all of which are good solar analogs, we returned to our original selection criteria and eliminated stars that would unbalance the bracketing of the Sun's properties (specifically HD 191854 and HD 30246). We ultimately accepted seven stars into our final subset, from the original 12 candidates, and these are indicated by boldface type in Table III and plotted with solid lines in Fig. 2. The colors from this subset were averaged, as listed at the end of Table V, and the results were adopted as representative solar colors. These colors compare very favorably to the solar analog colors used in the IHW system (Osborn *et al.* 1990) when they are both normalized to a common wavelength. Ultimately, these colors are used in the comet reduction procedures to represent the Sun for determining the spectral reflectivity of the dust (when the necessary continuum points were measured) or for a first approximation to the continuum color (if some continuum measurements are missing). It should be noted that, although we did not include all of our solar analogs into our average, they are all very close to the Sun in their properties and spectra and can probably be reliably used to represent the Sun in other observing programs. If wavelengths below 4000 Å are to be measured, however, care should be exercised with HD 11131 and HD 81809 (and possibly HD 217014) because they exhibit the largest deviations from the group as a whole.

3.2. Flux Standards

The selection of stars to be included in a standard star system always requires compromises, and comet flux standards are

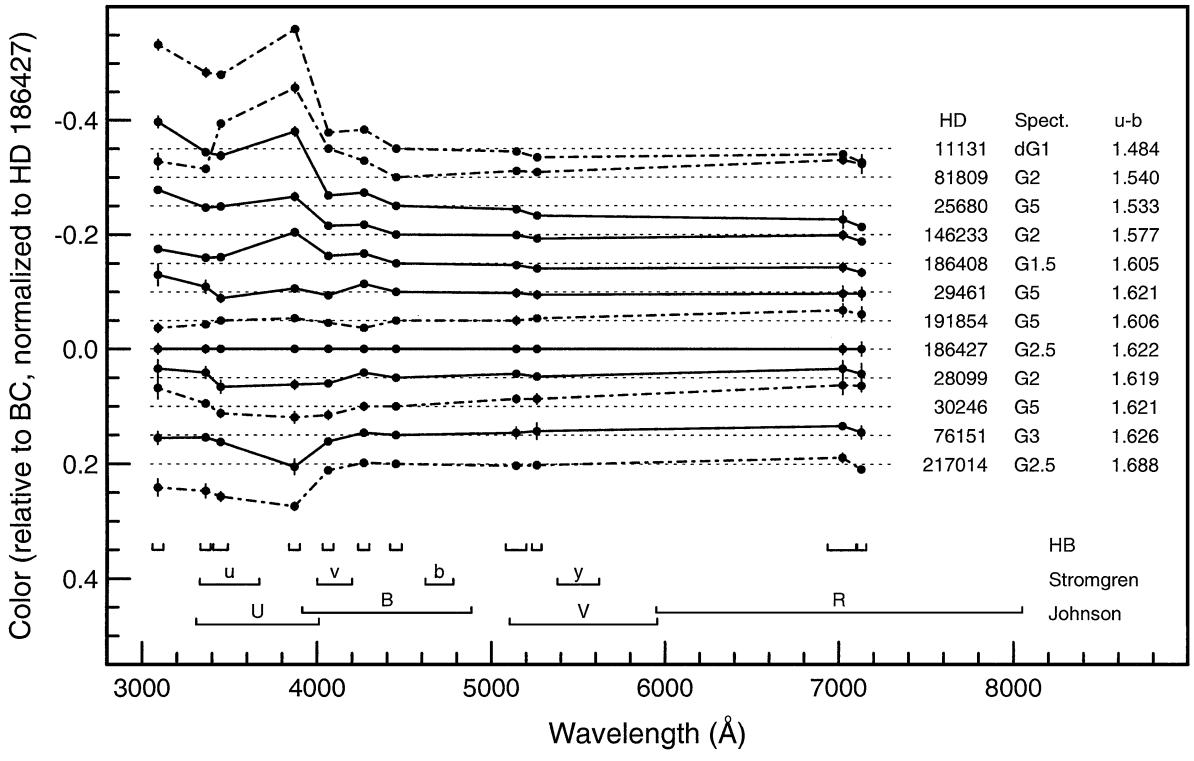

FIG. 2. Colors of the solar analogs, relative to the blue continuum (BC) filter and normalized to HD 186427. The plots are placed in order of their CN–BC color, with zero points offset for clarity. Dot–dash lines indicate stars that were not included in the final subset of solar analogs. If not shown, error bars lie within the points. At the bottom, the HB filter bandpasses are shown, along with the Strömgren uvby and Johnson UBVR filters for comparison. Strömgren u–b colors provide a useful discriminator when evaluating solar analogs (see text).

no exception. In addition to needing stars that exhibit little or no variability and have relatively strong UV flux, few spectral features, and an appropriate brightness for the instrumentation, one also desires that the stars have a similar airmass as the target comet. The previous comet standard systems included about a dozen B-type stars, most within 20° of the equator and having magnitudes ranging from 1.9 to 7.9. This guaranteed that an accessible star would match a comet's airmass within 1–2 h of the comet observation, although sometimes the star was too bright or faint to use effectively. Note that most of these primary flux standards were, in fact, the same stars, carried over from one filter system to the next. In the case of the IHW filter set, a supplemental or secondary set of stars, located along Halley's path during its 1985/86 apparition, was also calibrated, but many of these have been of little use in subsequent years. Finally, years of experience reducing comet photometry have shown that, for most circumstances, the most important criteria in picking specific stars for measuring extinction and instrumental corrections on a given night is the ability to match the range of airmasses traversed by the comet(s).

In an attempt to best utilize the earlier standard systems and to improve their overall effectiveness, we ultimately decided on a set of flux standards, again situated near the celestial equator, but with a higher density and a more regular mix of brightnesses. As a starting point, and following earlier practices, the IHW primary flux standards were adopted as HB standards (with the exception of HD 120315, which is too bright for most uses). These stars have been well-studied and shown to be acceptable as flux standards, and their adoption gave an immediate set of standards that could be used while additional stars were being evaluated. Furthermore, inclusion of the IHW primary stars as HB standards provides a means of comparing the old and new filter systems. Additional stars (late O or early B type) were then needed to fill in gaps in right ascension. Because so many large-format HB filters were manufactured for use in CCD imaging, we also decided to include standards at two different brightness tiers: a bright tier ($4.5 < V < 6.5$) to produce a high signal-to-noise in photometers and a fainter tier ($6.5 < V < 8.5$) to minimize the saturation of CCDs. The faint limit was set so that the stars are observable by most telescopes, yet are still bright enough for high signal-to-noise calibration using a photometer. In our selection of new stars, we also tried to avoid known variable stars, emission-line stars, and stars with known close companions.

To meet these criteria, we explored numerous catalogs of stars (e.g., Breger 1976, Goy 1980, Gunn and Stryker 1983, Stone 1977) searching for O or B stars within each brightness tier at intervals of 1.5 to 2 h in right ascension. The declination was also restricted to within 15° of the equator so that all of the stars are accessible to both the northern and southern hemispheres and so it is easier to predict the time at which a particular star

TABLE IV
Standard Star Magnitudes

Object	Magnitudes / Sigmas / Number of Observations										
	3090	3362	3448	3870	4062	4266	4450	5141	5260	7020	7128
Flux Standards											
HD 3379	5.650	5.673	5.680	5.716	5.714	5.713	5.717	5.728	5.727	5.749	5.748
53 Psc	0.018	0.014	0.014	0.010	0.008	0.010	0.007	0.008	0.008	0.013	0.011
	12	12	12	12	12	12	12	12	12	3	3
HD 6815	7.935	7.869	7.838	7.383	7.233	7.205	7.172	7.173	7.167	7.119	7.124
	0.017	0.013	0.010	0.010	0.008	0.007	0.010	0.008	0.009	0.011	0.002
	8	8	8	8	8	8	8	8	8	3	3
HD 14951	5.630	5.606	5.594	5.411	5.364	5.358	5.344	5.344	5.346	5.324	5.327
	0.021	0.023	0.020	0.014	0.012	0.011	0.011	0.009	0.011	0.003	0.003
	7	7	7	7	7	7	7	7	7	3	3
HD 19712	8.215	8.110	8.039	7.505	7.321	7.283	7.208	7.228	7.248	7.133	7.135
	0.013	0.015	0.014	0.008	0.009	0.006	0.011	0.006	0.006	0.006	0.013
	7	7	8	8	7	7	7	7	7	3	3
HD 26912	4.407	4.376	4.357	4.239	4.231	4.224	4.204	4.155	4.145	—	—
μ Tau	0.014	0.012	0.015	0.014	0.013	0.008	0.012	0.011	0.011	—	—
	11	11	12	12	12	11	12	12	13	—	—
HD 31331	6.018	6.004	6.003	5.875	5.856	5.848	5.838	5.837	5.836	5.807	5.810
	0.014	0.013	0.009	0.007	0.006	0.007	0.005	0.006	0.007	0.006	0.006
	14	14	14	14	14	15	14	14	14	5	5
HD 37112	8.167	8.147	8.134	7.976	7.914	7.899	7.881	7.867	7.863	7.814	7.803
	0.013	0.014	0.010	0.010	0.009	0.010	0.009	0.009	0.006	0.004	0.004
	7	7	7	7	7	7	7	7	7	5	5
HD 52266	6.838	6.850	6.833	7.129	7.246	7.219	7.195	7.093	7.073	6.933	6.917
	0.017	0.012	0.009	0.008	0.009	0.009	0.007	0.010	0.009	0.007	0.004
	8	9	11	11	11	9	11	11	11	3	4
HD 68099	6.366	6.325	6.297	5.986	5.948	5.947	5.921	5.931	5.931	5.898	5.901
	0.0173	0.009	0.009	0.007	0.008	0.007	0.009	0.007	0.007	0.014	0.006
	12	12	12	12	12	12	12	12	12	5	5
HD 72526	9.004	8.879	8.821	8.121	7.913	7.870	7.822	7.796	7.793	7.689	7.679
	0.014	0.009	0.009	0.008	0.008	0.009	0.007	0.008	0.008	0.008	0.006
	10	10	10	10	10	10	10	10	10	5	5
HD 74280	3.934	3.963	3.967	4.047	4.078	4.093	4.090	4.125	4.131	—	—
η Hya	0.015	0.010	0.009	0.010	0.009	0.008	0.009	0.007	0.008	—	—
	15	13	16	17	17	13	17	17	17	—	—
HD 89688	6.592	6.563	6.556	6.535	6.577	6.567	6.556	6.515	6.507	6.463	6.463
23 Sex	0.014	0.008	0.009	0.009	0.008	0.006	0.007	0.007	0.010	0.006	0.003
	13	10	13	13	13	11	14	14	14	4	5
HD 97991	6.718	6.779	6.796	7.081	7.164	7.173	7.186	7.225	7.230	7.317	7.311
	0.007	0.007	0.009	0.009	0.010	0.007	0.007	0.006	0.009	0.009	0.006
	8	8	8	8	8	8	8	8	8	5	5
HD 120086	7.414	7.444	7.460	7.619	7.664	7.669	7.680	7.698	7.702	7.764	7.766
	0.014	0.009	0.008	0.007	0.008	0.007	0.007	0.006	0.008	0.003	0.007
	12	8	12	12	12	8	12	11	11	4	5
HD 129956	6.637	6.523	6.476	5.808	5.652	5.612	5.573	5.546	5.544	5.440	5.431
	0.008	0.009	0.009	0.009	0.008	0.008	0.007	0.009	0.008	0.013	0.002
	9	7	9	9	9	7	9	9	9	4	4
HD 149363	7.536	7.517	7.504	7.748	7.858	7.822	7.784	7.658	7.638	7.474	7.448
	0.012	0.003	0.008	0.008	0.009	0.007	0.007	0.007	0.009	0.011	0.004
	10	5	10	10	10	5	10	10	10	2	2
HD 154445	5.822	5.729	5.708	5.813	5.841	5.791	5.754	5.556	5.520	5.203	5.191
	0.013	0.009	0.009	0.007	0.008	0.009	0.007	0.008	0.008	0.012	0.005
	11	7	11	11	11	7	11	11	11	4	4
HD 164852	5.207	5.200	5.188	5.166	5.149	5.144	5.133	5.114	5.108	5.052	5.054
96 Her	0.016	0.013	0.011	0.011	0.009	0.009	0.009	0.008	0.009	0.011	0.008
	22	14	22	23	23	14	23	23	23	5	6

TABLE IV—*Continued*

Object	Magnitudes / Sigmas / Number of Observations										
	3090	3362	3448	3870	4062	4266	4450	5141	5260	7020	7128
HD 170783	8.645	8.477	8.428	8.029	7.979	7.925	7.861	7.656	7.624	7.303	7.285
	0.017	0.009	0.009	0.009	0.007	0.008	0.009	0.010	0.008	0.007	0.006
	12	10	12	12	12	10	12	12	12	6	6
HD 187350	8.270	8.153	8.110	8.252	8.317	8.278	8.241	8.078	8.037	7.720	7.703
	0.018	0.009	0.013	0.013	0.013	0.011	0.012	0.013	0.010	0.021	0.019
	9	8	9	9	9	8	9	9	9	4	4
HD 191263	6.190	6.190	6.190	6.190	6.190	6.190	6.190	6.190	6.190	6.190	6.190
	0.012	0.010	0.011	0.007	0.007	0.008	0.006	0.005	0.005	0.006	0.005
	16	13	16	16	16	13	16	16	16	6	6
HD 205130	8.375	8.314	8.286	7.868	7.799	7.780	7.752	7.742	7.740	7.682	7.684
	0.012	0.010	0.007	0.007	0.004	0.006	0.005	0.006	0.006	0.008	0.008
	9	9	9	9	9	9	9	9	9	3	4
HD 209008	6.003	5.991	5.981	5.872	5.876	5.876	5.862	5.850	5.848	5.813	5.815
	0.012	0.009	0.007	0.007	0.005	0.006	0.005	0.002	0.006	0.006	0.002
	12	10	12	12	12	10	12	12	12	4	4
HD 219188	6.481	6.516	6.514	6.820	6.956	6.947	6.932	6.917	6.909	6.885	6.884
	0.015	0.011	0.012	0.008	0.009	0.006	0.006	0.005	0.006	0.006	0.004
	11	9	11	11	11	9	11	11	11	3	3
Solar Analogs											
HD 11131	8.870	8.298	8.207	8.068	7.692	7.537	7.220	6.802	6.724	5.981	5.960
	0.015	0.013	0.005	0.005	0.006	0.010	0.007	0.007	0.009	0.019	0.011
	8	8	8	6	6	6	6	8	6	2	2
HD 25680	8.063	7.495	7.406	7.305	6.859	6.704	6.377	5.960	5.883	5.152	5.130
39 Tau	0.017	0.010	0.012	0.011	0.009	0.008	0.010	0.009	0.008	0.010	0.012
	10	8	10	10	10	8	10	10	10	4	4
HD 28099	10.419	9.805	9.736	9.673	9.113	8.944	8.603	8.173	8.090	7.338	7.312
vB 64	0.020	0.023	0.021	0.016	0.017	0.020	0.015	0.013	0.016	0.012	0.015
	7	6	8	8	8	6	8	8	8	2	2
HD 29461	10.254	9.654	9.579	9.503	8.957	8.787	8.451	8.030	7.945	7.205	7.170
vB 106	0.013	0.007	0.011	0.011	0.010	0.003	0.010	0.006	0.006	0.006	0.008
	6	5	6	6	6	5	6	6	6	3	3
HD 30246	10.647	10.054	9.976	9.924	9.362	9.197	8.847	8.411	8.323	7.561	7.527
vB 142	0.016	0.006	0.011	0.013	0.010	0.010	0.008	0.009	0.008	0.006	0.012
	6	6	7	7	7	6	7	7	7	4	4
HD 76151	8.339	7.717	7.630	7.614	7.012	6.847	6.501	6.074	5.983	5.236	5.212
	0.006	0.006	0.014	0.019	0.013	0.007	0.013	0.006	0.009	0.005	0.008
	6	5	8	9	9	5	9	9	9	3	4
HD 81809	7.671	7.063	6.889	6.767	6.316	6.187	5.866	5.432	5.346	4.587	4.559
	0.009	0.004	0.006	0.012	0.007	0.003	0.006	0.005	0.004	0.013	0.013
	5	5	6	7	7	5	7	7	7	3	4
HD 146233	7.736	7.145	7.048	6.972	6.465	6.313	5.980	5.558	5.476	4.732	4.708
18 Sco	0.009	0.009	0.007	0.010	0.007	0.009	0.006	0.009	0.008	0.006	0.004
	5	5	5	5	5	5	5	5	5	4	4
HD 186408	8.267	7.661	7.565	7.463	6.946	6.792	6.459	6.039	5.957	5.217	5.191
16 Cyg A	0.008	0.009	0.005	0.005	0.005	0.009	0.005	0.007	0.008	0.013	0.007
	9	7	9	9	9	7	9	9	9	4	5
HD 186427	8.558	7.937	7.842	7.783	7.225	7.075	6.725	6.302	6.214	5.476	5.441
16 Cyg B	0.011	0.008	0.005	0.005	0.004	0.009	0.005	0.007	0.009	0.009	0.007
	9	7	9	9	9	7	9	9	9	4	4
HD 191854	9.755	9.128	9.026	8.963	8.413	8.272	7.909	7.486	7.394	6.642	6.614
	0.009	0.005	0.005	0.009	0.003	0.003	0.003	0.008	0.005	0.012	0.009
	7	6	7	7	7	6	7	7	7	4	4
HD 217014	7.817	7.202	7.117	7.075	6.454	6.291	5.943	5.523	5.434	4.683	4.668
51 Peg	0.018	0.015	0.012	0.011	0.007	0.008	0.005	0.007	0.006	0.009	0.005
	9	9	9	9	9	9	9	9	9	4	4

TABLE V
Solar Analog Colors

Object	Other name	Colors relative to BC										
		3090	3362	3448	3870	4062	4266	4450	5141	5260	7020	7128
HD 25680	39 Tau	1.686	1.118	1.029	0.928	0.482	0.327	0.000	−0.417	−0.494	−1.225	−1.247
HD 28099	vB 64	1.817	1.203	1.133	1.070	0.510	0.341	0.000	−0.430	−0.513	−1.265	−1.291
HD 29461	vB 106	1.803	1.203	1.128	1.052	0.506	0.336	0.000	−0.421	−0.506	−1.246	−1.281
HD 76151		1.838	1.216	1.129	1.113	0.511	0.346	0.000	−0.427	−0.518	−1.265	−1.289
HD 146233	18 Sco	1.755	1.165	1.068	0.992	0.485	0.333	0.000	−0.422	−0.504	−1.248	−1.272
HD 186408	16 Cyg A	1.808	1.202	1.106	1.004	0.487	0.333	0.000	−0.420	−0.502	−1.242	−1.268
HD 186427	16 Cyg B	1.833	1.212	1.117	1.058	0.500	0.350	0.000	−0.423	−0.511	−1.249	−1.284
Average		1.791	1.188	1.101	1.031	0.497	0.338	0.000	−0.423	−0.507	−1.249	−1.276

will be at a given airmass. Due to the lack of early-type stars far from the galactic plane, we were not always able to satisfy all of the criteria we set. Several late B-type stars were accepted to improve the coverage in right ascension, yet even with these additions, there are gaps as large as 2.5 h and regions where only a faint-tier star is available. Also, several stars have exhibited a slight variability ($\Delta m < 0.05$ mag, e.g., Kholopov *et al.* 1981, Skiff 1994), but these are all IHW standards that have been used for many years with no evident problems. In all, 24 stars were selected, and a list of the stars, their coordinates, V magnitudes, spectral types, and colors are given in Table II, and their distribution on the sky is shown in Fig. 3.

4. ESTABLISHING THE STANDARD STAR MAGNITUDE SYSTEM

The second step in establishing the standard star system is to observe each star and, using these measurements, to establish a magnitude system for the HB filters. Because these magnitudes are critical for the absolute calibration of data, extreme care was taken to ensure that conditions were sufficient for obtaining high-quality data. First, as was stated in Section 2, a filter set whose transmission characteristics are representative of the average of all of the filters was used to obtain the data so that the results would apply to all filter sets. Second, to ensure uniformity of the data, all measurements were obtained at one site, primarily with a single photoelectric photometer (though a CCD was used to acquire necessary measurements at red wavelengths). Third, each star was observed on as many scheduled nights as possible over a 16-month period to provide extensive coverage. Finally, reduction of the data and its incorporation into a magnitude system were both carefully performed, with consistency checks throughout to look for any problem data sets.

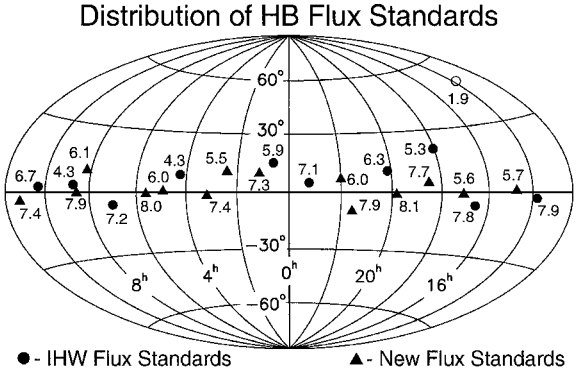

FIG. 3. Distribution, in right ascension and declination, of the HB flux standards. Filled circles are stars that were adopted from the primary IHW standards, triangles are new stars that were added, and the open circle is the IHW primary that was rejected due to its brightness. The V magnitude for each star is given next to its symbol.

4.1. Standard Star Observations

To ensure uniformity of the data, all observations were obtained at Lowell Observatory, using either the 31-in. (0.8-m) or the 42-in. (1.1-m) Hall telescope. Furthermore, for nine of the 11 filters (OH through GC) all observations were made with a single photoelectric photometer with pulse counting electronics, the same photometer that has been used in comet studies at Lowell Observatory for two decades. A photometer was used for several reasons: data can be obtained more rapidly than with a CCD, due to less overhead; the photometer has a higher signal-to-noise; and using a single photometer for all of the data in the nine filters avoids problems associated with different observers and instruments (Osborn *et al.* 1990). Unfortunately, the sensitivity of this high-UV throughput phototube drops off to near-zero by 6500 Å, so it could not be used to calibrate the two red HB filters. Out of necessity, therefore, the data used to calibrate the H_2O^+ and RC filters were obtained using a 2048×2048 Site CCD with 2×2 binning. To tie these data to the photometer results, CCD measurements were obtained with filters from CN through GC as well as with H_2O^+ and RC. A comparison of the data from these overlapping filters indicates that the final CCD magnitudes are completely consistent with those from the

photometer, though with larger uncertainties. The match was good enough (within 1σ) that no corrections were needed to adjust for the different instruments. Because of their lower signal-to-noise, however, the CCD measurements obtained with the overlapping filters were not included in the final magnitude determinations.

Standard star observations spanned a period of 16 months (January 1997 through April 1998), at approximately monthly intervals. A set of data consists of a sequence of observations of a star with all of the available filters and between seven and 37 sets were obtained each night, with an average of 22 sets (not including high airmass extinction measurements). Data from nights later determined to be non-photometric were discarded, which left 18 out of 24 nights of photometry and seven out of eight nights of CCD measurements to be included. Each star was observed as frequently as possible, resulting in five to 11 nights of photometry and two to four nights of CCD data for each star. Two stars, HD 26912 and HD 74280, were too bright to observe with the CCD, even with defocussing of the image to spread out the light, and so no measurements were obtained for these stars with the H_2O^+ or RC filters.

4.2. Data Reduction

Basic reduction of the standard star data followed normal procedures. In the case of the photometer, the raw counts were corrected for the dead time of the phototube, and then the sky background, measured nearby, was subtracted. For the CCD, the bias level was removed from each image, which was then flat fielded using twilight sky flats to remove the pixel-to-pixel variations. Aperture photometry was done with IDL photometry routines, using an aperture large enough to measure the light from the star out to the point where noise became a significant issue. Because some of the stars needed to be defocussed to keep them from saturating, different-sized apertures were used; however, a constant-sized aperture was used for each level of defocussing. The sky background was determined from an annulus around the aperture and subtracted from the total counts within the aperture. The measured counts from both the CCD and the photometer were then converted to instrumental magnitudes before correcting for atmospheric extinction.

The extinction was carefully determined for each night, using at least two stars observed at a series of different airmasses. The airmass was determined from Hardie's (1962) approximation, with a correction for the elevation effect in the apparent zenith angle. (This is discussed in more detail, and the equations are given, in Appendix A.) We assume that the extinction of an object (in magnitudes) varies linearly with airmass, a good assumption for all filters except OH which will be discussed next. If more than one extinction star was measured, then the average extinction coefficient among the stars was used for each filter. As a check on the extinction solution, and to allow adjustments to the coefficients found from poorly determined extinction stars, a global solution was used. In this situation, the coefficients were adjusted so as to minimize the variations between the Δms (difference between the instrumental and HB magnitude) for measurements of all of the stars. Note that this could only be done in the re-reduction of the data, after preliminary magnitudes had been determined as discussed below. These global solutions were used on the few nights where the Δms were significantly improved over the original extinction solution, otherwise the original extinction star coefficients were kept for the final reductions.

Unfortunately, a linear extinction coefficient could not be used for the OH filter. Plots of observed OH magnitude versus airmass produce a curve, rather than a line, and forcing a linear fit to measurements along this curve gave discrepant magnitudes when the individual points were extrapolated to zero airmass. Furthermore, the extrapolated results would change if a different range of airmass was used, because a different part of the curve was being fit. Therefore, it was necessary to use models of atmospheric extinction to reproduce the curvature in the magnitude–airmass plot so that a proper extrapolation to zero airmass could be done, regardless of the range of airmass at which the data were obtained.

A series of tests were performed, in which synthetic spectra (representing B stars, G stars, and comets) were convolved with various extinction functions, to explore how those functions affect measurements at different airmasses and to determine what aspects of the extinction function introduce the curvature into the magnitude–airmass relation. The results of these tests proved that the majority of the curvature is produced by the slope of the extinction function, with the steepness related to the amount of curvature produced. (A slope that decreases with wavelength produces a redward shift in the effective central wavelength of the flux, because the blue light is removed more rapidly than the red. As airmass increases, the rate of this shift is initially very rapid, but slows at higher airmass because the edge of the filter bandpass limits the amount of shift that can be produced. The curvature in the magnitude–airmass relation is a result of the fact that the rate of this shift changes with airmass.) In addition, if the extinction curve itself is not linear, but has a changing slope across the bandpass, then this will also contribute to the curvature, though at a much lower level than from the slope. The OH extinction tests also proved that the color of the object has only a minor influence on the results, when compared to the extreme effect of variable extinction across the bandpass. Consequently, the extinction can be treated with the same formulation for B and G stars, as well as comets. However, because of the different spectral shapes of these objects, the coefficients within that formulation will be different for each type of object.

The OH extinction tests also showed that the three primary components of extinction—Rayleigh scattering, aerosols, and ozone—could be addressed individually, without changing the final result. The specific procedures used to determine the extinction in the OH filter are outlined in Appendix A. As shown there, analysis of the extinction star measurements produces not

just one linear extinction coefficient, but rather separate measures of the contribution from aerosols and the amount of ozone present. These quantities, when combined with a calculation of the Rayleigh contribution, are used to reproduce the proper curvature for extrapolating to zero airmass.

The extinction coefficients (and for OH, the aerosol and ozone measurements) were then used to correct each individual data point to its value above the atmosphere, giving the instrumental magnitude of each measurement. Once the instrumental magnitudes have been determined for each measurement, they are used to establish the HB magnitude systems (cf. Osborn *et al.* 1990).

4.3. Computing Standard Star Magnitudes

Although not discussed at length in this paper, colors played an important role in the analysis of the standard stars and, ultimately, as a consistency check in the establishment of the magnitude system. The standard stars all have different magnitudes, so colors are used as a straightforward means of comparing and contrasting them (as was already seen in the discussion of solar analogs). During the calibration process, we defined a *fundamental filter* to be a basis from which colors are normally calculated. The BC (4450 Å) filter was selected as our fundamental filter for several reasons: it can be used to obtain a good signal-to-noise with both the photometer and the CCD; it is near the center wavelength of the basic (CN through GC) filters, which were most requested by filter recipients; it is near the center of the Johnson B bandpass (the significance of which is discussed in the next paragraph); and finally, the atmospheric extinction at 4450 Å is fairly low, reducing uncertainties introduced by extrapolating a measurement to zero airmass. Unless otherwise stated, colors in the HB system are given relative to this filter (e.g., $m_{\rm OH} - m_{\rm BC}$).

Another fundamental in the calibration procedures is the fundamental star, which is important because it is the standard upon which all other HB magnitudes are based. The magnitudes for this star are set at a predefined value for each filter, and the magnitudes of all the other stars are computed relative to those values. We selected HD 191263 as our fundamental star, primarily because it is in the middle range of brightness and so can be observed with both the photometer and the CCD, and it is an IHW standard, so a direct comparison can be made between the two filter systems. In addition, it was available at the start of our observing campaign, which allowed preliminary results to be computed. While the pre-defined magnitudes of the fundamental star are somewhat arbitrary, the conversion to absolute fluxes (addressed in Section 5) directly accounts for any particular magnitude that is selected. Because BC is the fundamental filter, we chose to set the BC magnitude of HD 191263 to 6.19, to match its Johnson B magnitude. Furthermore, to make the fundamental star easy to identify in lists or plots and to follow the convention established with the earlier comet filter sets, the same value was assigned to all of the filters, meaning that it exhibits no color in the HB system. Using the pre-set magnitudes for HD 191263 as a starting point, an iterative process was then used to determine the magnitudes of the other stars. A detailed description of this process is given in Appendix B. As is described there, we were careful throughout the procedure to not allow the fundamental star to receive a greater weighting than other stars in establishing the magnitude system. In addition to computing the magnitudes directly, a consistency check was performed by using colors to compute the magnitudes indirectly. Both procedures gave essentially identical results, but the magnitudes from the direct computation were ultimately adopted, due to slightly better uncertainties. (The errors on the colors tended to be quite small, but when converting colors to magnitudes, incorporation of the uncertainty on the BC magnitude typically raised the overall errors to equal or higher than those for the magnitudes determined directly.)

The final magnitudes for both the solar analogs and the flux standards are given in Table IV and the final colors of the solar analogs are listed in Table V (and were discussed in Section 3.1). Table IV also lists the number of observations that were included in the average for each star. The uncertainties in the magnitudes are typically around 0.007 at wavelengths above 4000 Å and increase in the UV where the signal is weaker. These values are comparable to the mean errors in the IHW magnitude determinations; however, our uncertainties are more consistent from star-to-star. This is due to the fact that all of the HB observations were obtained at Lowell Observatory, and a roughly equal number of measurements were obtained for each star, whereas in the IHW system, observations were collected from many sources (using different instruments) and the magnitudes were computed using anywhere from one to 119 measurements (Osborn *et al.* 1990).

To intercompare the results from the different flux standards, their colors are plotted in Fig. 4. The stars are placed in a sequence defined by their UC–C_3 color, which spans the Balmer discontinuity. This sequence was chosen primarily for clarity, but it also permits a search for correlations between the star's spectral type and its colors. Another practical reason for looking specifically at the UV colors was to determine which stars might be affected by any color terms in the OH extinction; this ultimately proved to be a non-issue for the HB filters, unlike the IHW filters, where color variations among the B stars do have an effect. It is immediately obvious from the plot that five stars are significantly reddened and one star is slightly reddened (dashed lines). Although four of these stars were previously known to be reddened (Delgado *et al.* 1997, Winkler 1997, Wolff *et al.* 1996), HD 187350 and HD 219188 are not listed as reddened in any of the catalogs that were explored (though the reddening may actually be the effects of metallicity or age). Placing these stars in order of their reddened UC–C_3 color would be misleading in searching for correlations, so we attempted to remove the effects of reddening to allow us to place the stars in their proper location in the sequence. Noting that the colors of the unreddened stars are all similar for wavelengths longer than 4500 Å, with a slight increase in slope toward later spectral type, we used this region

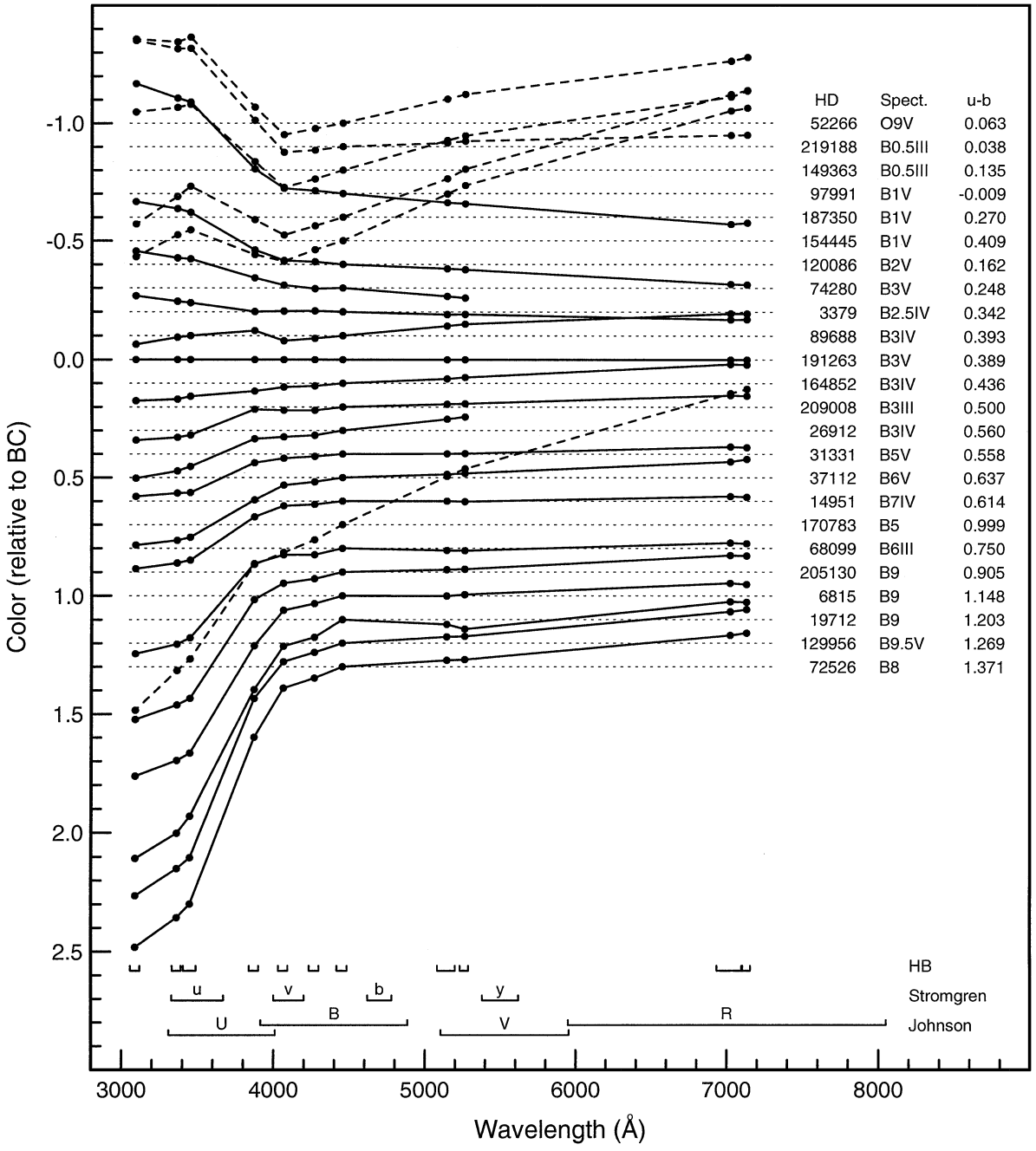

FIG. 4. Colors of the flux standards, relative to the blue continuum (BC) filter. The curves are placed in order of their de-reddened UC–C_3 color, with zero points offset for clarity. The zero level for each star is denoted by the horizontal dotted line, with the BC filter at 4450 Å always located at zero. HD 191263 is defined to have magnitude 6.19 in all filters, so it has no color, and the red magnitudes of HD 26912 and HD 74280 were not determined because of the stars' brightness, so there are no corresponding colors for those filters. The dashed lines indicate stars that exhibit significant reddening. The error bars fall within the point size.

to apply a first order correction to the UC–C_3 color. Assuming that, to first order, the reddening is constant with wavelength, we corrected the RC–BC segment so its slope matched the slope of its unreddened neighbors, and then scaled this adjustment to the UC–C_3 segment. This correction works well for the purpose of ordering the stars, because the UC–C_3 color differences are large enough that small errors in the assumed RC–BC slope will not affect the star's position in the plot.

The resulting sequence exhibits a range of 1.5 mag in the near-UV colors, clearly showing how the strength of the Balmer discontinuity and the flux at shorter wavelengths changes from early- to late-type B stars. On the other hand, at wavelengths

above 4500 Å, all B-type stars tend to have very similar color characteristics. The UV results suggest that the UC–C_3 index is extremely sensitive to the temperature of the star, in which case it may be useful as a tool to help in pinpointing the spectral type. Looking specifically at the UV colors in Fig. 4, it appears that HD 68099, which is classified as a B6 star, but also has entries for B7 and B8 in the Simbad database, should actually be closer to B8. Similarly, HD 72526, which has the largest color extreme of all of our standards, should be type A0 or A1, rather than B8. Comparing our UC–C_3 sequence with the Strömgren u–b color also produces a very close correlation (for the non-reddened stars), suggesting that, again, the u–b color can be used as a discriminator for the initial evaluation of other B stars.

5. CALIBRATION OF THE FILTERS

The procedures for reducing comet data are similar, regardless of which narrowband comet filter set was used for the observations: standard star information (discussed in Appendix C) is used to convert the measured count rates into absolute fluxes; gas contamination is removed from the continuum measurements (in an iterative process); underlying continuum is removed from the gas measurements; and finally, the measured fluxes are converted to a total band flux, if that is what is ultimately desired. In the past, these tasks were dealt with individually on a filter-by-filter basis that did not account for the mutual contaminations of two species (which may have been due, in part, to the fact that some of the contaminations were unknown at the time of the calibrations). While developing the general reduction procedures for the HB systems, we employed a new formalism in which one equation format applies to all species and can be solved for mutual contaminations in any combination of filters. The following sections provide a brief account of the filter calibration process, in which we developed the new formulation, derived the equations and computed the coefficients that will ultimately be used for reducing comet data. Furthermore, during the calibration process, we performed a series of tests to measure how the coefficients are affected by variations in the filters and in observing conditions. The results of these tests and their implications on the data reduction process are given. In the generalized notation used here, XX and YY represent any of the filter species (OH, NH, UC, etc.).

5.1. *Derivation of Reduction Coefficients*

Because most observers will use a subset of the 11 HB filters, procedures for the reduction of comet data should be able to account for continuum measurements at any sensible combination of the four wavelengths and still produce results that can be compared to other observers (who potentially used a different combination of filters). We have established a basic set of procedures that we feel provides the best reduction of comet data for the variety of situations that may be encountered. Appendix D details these procedures in a step-by-step outline and gives the relevant equations that are needed for reducing comet data. The reduction coefficients that are used in these equations are related to the filter bandpasses and spectral bands that are being measured. The following discussion introduces and defines the various coefficients, addresses any factors that were considered during their derivation, and describes how they fit into the data reduction process.

The first coefficient, $F_{0_{XX}}$, is the absolute flux of a 0 magnitude star in the HB system. It is used to convert an HB magnitude to an absolute flux, using the familiar equation

$$F_{XX} = F_{0_{XX}} 10^{-0.4 m_{XX}}, \tag{1}$$

where m_{XX} is the HB magnitude. We determined the values for these coefficients using the fluxes for several HB standards listed in spectrophotometric star catalogs and tied them to an absolute system through the Hayes and Latham (1975) flux for Vega at 5556 Å. The details concerning the computation of these flux conversion coefficients are given in Appendix C. The second coefficient, the solar color $m_{\odot XX}$, is the adopted color of the solar spectrum and, as discussed in Section 3.1, is used for dealing with the continuum filters. The values for both $F_{0_{XX}}$ and $m_{\odot XX}$ are listed in Table VI.

When measured data are going to be extrapolated to total band fluxes, it is critical to understand what fraction of each emission band was actually captured by a filter. The third coefficient, γ (or alternatively, γ'), is a measure of this fraction. To compute these values, we used a representative emission line spectrum (either synthetic or measured from a comet with the appropriate emission features) for each of the species of interest. Whenever possible, synthetic spectra were used for the calibrations, because there are no problems associated with continuum subtraction or contamination from other species, they are not adversely

TABLE VI
Filter Calibration Coefficients

Species[a]	F_{0XX}[b]	$m_{\odot XX}$	$\gamma_{XX/XX}$	$\gamma'_{XX/XX}$
OH	10.560	+1.791	1.698×10^{-2}	0.98
NH	8.420	+1.188	1.907×10^{-2}	0.99
CN	8.6	+1.031	1.812×10^{-2}	0.99
C_3	8.160	+0.497	3.352×10^{-3}	0.19
CO^+	7.323	+0.338	1.549×10^{-2}	0.99
C_2	3.887	−0.423	5.433×10^{-3}	0.66
H_2O^+	1.380	−1.249	5.424×10^{-3}	1.00
UC	7.802	+1.101	—	—
BC	6.210	0.000	—	—
GC	3.616	−0.507	—	—
RC	1.316	−1.276	—	—

[a] Filter specification represented by XX subscript.
[b] Flux of 0 magnitude star (10^{-9} erg cm^{-2} s^{-1} Å^{-1}).

affected by instrumental resolutions that can affect measured spectra, and they can be generated for a variety of situations (different heliocentric velocities, distances, etc.), which helps in evaluating how the final coefficients are affected by changing conditions. We were able to obtain synthetic spectra for OH, NH, and CN (from Schleicher and A'Hearn (1988), Meier (1998), and Schleicher (1983), respectively), each of which was generated for different velocities and distances, if appropriate. For the other species, we explored the available synthetic spectra (e.g., C_2 from A'Hearn (1978), C_3 from Kim (personal communication, 1998)); however, these were unsuitable for our purposes. Instead, we used high-quality comet spectra, from which the sky, continuum, and any emission lines contaminating the desired species were removed. Whenever possible, we extracted representative spectra at different distances from the nucleus, to evaluate the quality of the continuum removal and to observe how the bandshapes changed with distance. The C_2 and C_3 bands were extracted from a spectrum of Comet deVico (A. Cochran, personal communication, 1998), the CO^+ is from a spectrum of Comet Schwassmann–Wachmann 1 (Cochran and Cochran 1991, Cochran *et al.* 1991), and the H_2O^+ band was extracted from Wehinger *et al.* (1974) and Wyckoff and Wehinger (1976).

To determine what fraction of an emission band passes through a particular filter, the spectrum is combined with the filter transmission profile. This technique is used not only to measure the emission from the desired species, but also to determine how much contamination from an undesired species is present, both in gas and in continuum filters. The quantities obtained in this manner are denoted here by the coefficient γ'. Specifically, $\gamma'_{XX/YY}$ is the fraction of the total emission band from species YY that is measured through filter XX,

$$\gamma' = \frac{\int f_{\lambda_{YY}} S_{\lambda_{XX}}\, d\lambda}{\int f_{\lambda_{YY}}\, d\lambda}, \tag{2}$$

where $f_{\lambda_{YY}}$ is the flux distribution in the emission band and $S_{\lambda_{XX}}$ is the transmission profile of the filter. Thus, $\gamma'_{\mathrm{CN/CN}}$ represents the fraction of the CN band that is measured through the CN filter, and $\gamma'_{\mathrm{CN/C_3}}$ is the fraction of the C_3 band that is contaminating the CN filter. A second coefficient, ultimately used in the reduction equations, is γ, which is simply γ' normalized by the filter's equivalent width and transmission properties:

$$\gamma = \frac{\int f_{\lambda_{YY}} S_{\lambda_{XX}}\, d\lambda}{\int f_{\lambda_{YY}}\, d\lambda \int S_{\lambda_{XX}}\, d\lambda}. \tag{3}$$

The relevant (non-zero) values of γ and γ' are listed in Tables VI and VII. Note that the measured fractions of the C_2 and especially the C_3 band listed for the HB filters are both smaller than the corresponding values quoted for previous filter sets, due to a better understanding of how broad the wings of these bands are. Although the HB coefficients differ substantially from the corresponding IHW values, in turn affecting the value of the total flux computed, the fluorescence efficiencies should, in principle, also change, to account for the additional lines within the total band. When the number of molecules is computed, the two effects will largely cancel each other out. The broad wings of C_3 also warrant another caution: C_3 contamination of NH, of CO^+, and especially of CN can be significant, because the wing contaminates the entire bandpass of these filters. In the case of CN, the integrated C_3 flux can comprise 10–15% or more of the total measurement, depending on the aperture size.

TABLE VII
Contamination Coefficients

Gas

Species[a]	γ_{XX/C_3}
NH/C_3	1.433×10^{-5}
CN/C_3	1.427×10^{-3}
CO^+/C_3	4.607×10^{-4}

Continuum

Species[a]	K_{XX1}	K_{XX2}	K_{XX3}
GC/C_2	0.0404	0.0348	0.0373
UC/C_3	0.0327	—	0.0293

[a] First species is represented by XX subscript; second species is the contaminant.

The new formalism for the HB filters (which will ultimately be applied back to the previous filter sets to improve corrections of continuum contamination) makes use of these γ coefficients in the generalized equation

$$\begin{aligned}\overline{F_{XX}} = {} & F_{\mathrm{OH}}\gamma_{XX/\mathrm{OH}} + F_{\mathrm{NH}}\gamma_{XX/\mathrm{NH}} + F_{\mathrm{CN}}\gamma_{XX/\mathrm{CN}} \\ & + F_{\mathrm{C_3}}\gamma_{XX/\mathrm{C_3}} + F_{(\mathrm{CO^+})}\gamma_{(XX/\mathrm{CO^+})} + F_{\mathrm{C_2}}\gamma_{XX/\mathrm{C_2}} \\ & + F_{(\mathrm{H_2O^+})}\gamma_{(\mathrm{XX/H_2O^+})} + \overline{F_{XX_{\mathrm{cont}}}},\end{aligned} \tag{4}$$

where $\overline{F_{XX}}$ is the wavelength averaged flux measured through the XX filter, $\overline{F_{XX_{\mathrm{cont}}}}$ is the average underlying continuum in filter XX, and F_{OH}, F_{NH}, etc., are the total band fluxes from each species and represent the final quantities that are to be determined. An equation of this form is written for each filter, and all 11 equations are solved simultaneously for the total band fluxes. (Note that an additional set of equations must also be utilized to interpolate between continuum filters for the underlying continuum in each gas filter.) By solving for all of the fluxes simultaneously, the contamination in each filter (from those species being measured) is accounted for. In cases where filter XX is not contaminated by species YY, the $\gamma_{XX/YY}$ terms are zero, simplifying the equations. In fact, for the HB filters, contaminations were minimized to the point that there are no mutually contaminating gas or ion filters, so the generalized simultaneous solution reduces to a straightforward linear series of relevant equations.

The last set of coefficients K_{XX1}, K_{XX2}, and K_{XX3}, are used for decontaminating the GC and UC filters, so the total flux from the continuum, $\overline{F_{XX_{\rm cont}}}$, can be determined. During the derivation of the reduction equations, several combinations of the F_0, $m_\odot$, and γ coefficients are produced, some of which are very complicated. To simplify the equations, we chose to present these combinations as individual constants, though they are discussed further in Appendix D. The relevant K coefficients are given in Table VII.

5.2. *Results of Coefficient Tests*

During the process of computing the γ coefficients, a series of tests were performed to determine how the calibrations are affected by factors that can change the emission spectrum or alter the filter transmission profile. Specific items that were examined include the effects of temperature, f-ratio, variations between filters produced in different evaporation runs, heliocentric distance and velocity, and, finally, variable extinction across the filter bandpass. Fortunately, the results of these tests indicate that, for typical observing conditions, most of these factors have no significant effect on the HB filter calibrations. Only two issues, small f-ratios and a few individual filters (as discussed below), produce a variation in the coefficients greater than 2 or 3%.

Changes in both temperature and f-ratio produce a change in the transmission profile of the filter, which in turn alters the particular region of the spectrum that is measured. In the case of the temperature, this change is a simple shift, claimed by the manufacturer to be

$$\Delta\lambda = 4 \times 10^{-6}\lambda \ (\text{per}\,^\circ\text{C}), \tag{5}$$

where the wavelength increases with increasing temperature. Thus, even a 30° temperature change in the RC filter causes a shift of less than 1 Å, so the effects of temperature can be neglected under all but extreme observing circumstances. The effect of the f-ratio, on the other hand, is dependent on the exact telescope system being used. For light entering the filter at an angle less than 90° to the face of the filter, the transmission profile shifts to the blue. With smaller f-ratios, light is entering at a smaller angle, and for that fraction of the light, the transmission profile shifts further blueward. Note, however, that even for a small f-ratio system, part of the light is passing through the filter at near 90°; thus, the effective filter transmission profile is the superposition of many different profiles, each shifted by a different amount. This change in the effective transmission profile is a concern because, with the increase in CCD usage, many telescopes are being operated at smaller f-ratios than in the past. As a compromise between typical f-ratios that might be used, the filters were optimized for use at approximately $f/6$, and the final coefficients were computed using this value, To test the effects of differing f-ratios, we performed a theoretical change of the filter bandpass for f/∞, $f/8$, $f/6$, $f/4$, and $f/3$ and combined the shifted bandpass with the emission spectra to observe how γ changed. For species in which the emission band is entirely within filter bandpass (OH, NH, CN, CO^+, and H_2O^+) different f-ratios have very little effect on γ, changing, at most, 2% over the range from f/∞ to $f/3$. However, for the wide bands of C_2 and C_3, shifting the transmission profile to the blue allows more of the emission band to pass through the filter, thus increasing γ. As it turns out, C_2 and C_3 both change by the same amount for the ratios tested, so that, relative to the nominal $f/6$ value, γ is 1.5% lower at f/∞, 1.8% higher at $f/4$, and 4% higher at $f/3$. For faster systems, the difference increases even more rapidly. The four continuum filters are situated clear of any significant emission features, so for ratios as small as $f/3$, there is no additional contamination beyond what was discussed earlier. In fact, there is a very slight drop, with decreasing f-ratio, in the level of contamination to the UC and GC filters because the bandpass is shifted farther out into the wing of the contaminating species.

Due to the nature of the manufacturing process, there will be slight variations in the transmission profiles of filters produced from one evaporation run to another. These differences can be in the central wavelength, the bandwidth, and/or the shape of the profile, which will in turn affect the coefficients. Fortunately, the run-to-run variations tend to be small, and for the vast majority of the filters, the error in the coefficients is less than 1–2%. However, there are a few C_2 and C_3 filters (mostly large format imaging filters) whose transmission profiles are shifted by up to 10 Å from our representative filter. Typically this will introduce a 3–5% error, with the worst of these cases causing an error of 10%. The recipients of these filters have been notified of the possible problem.

The next series of tests evaluated effects due to the comet's heliocentric distance and velocity. The heliocentric distance determines the amount of solar insolation that is available to excite the gas molecules, while, through the Swings effect (Swings 1941), the heliocentric velocity alters the distribution of the species' emission lines. Because both of these factors alter the relative line intensities within the emission band, they may also produce changes in the calibration coefficients. The OH, NH, and CN spectra were tested for velocities from -60 to $+60$ km s^{-1} and for distances from 0.5 to 5.66 AU to observe how the calibration coefficients changed. The maximum variation in γ is less than 2% for all situations, reflecting the fact that all three of these filters were designed to capture the entire emission band within the flat top of the filter profile. At heliocentric distances smaller than 0.5 AU, however, the variation in $\gamma_{\rm CN/CN}$ continues to increase, reaching 10% at 0.25 AU. This should rarely be an issue, though, because the minimum practical solar elongation for observing a comet is usually about 30°, which corresponds to a minimum heliocentric distance of 0.5 AU. For C_2 and to a lesser extent C_3, the spectrum exhibits differences with respect to heliocentric distance due to the different number of rotational levels populated and, with projected distance from the nucleus, due to the changing rotational levels populated as the molecules reach fluorescence equilibrium. We used several observed spectra to determine what the best typical bandshape for each species

was, and the deVico spectrum that was used reflects this shape. For the remaining species (CO^+ and H_2O^+), the effects of heliocentric velocity and distance are significantly smaller than for the species discussed above.

Finally, the atmospheric extinction in the UV changes so rapidly with wavelength that there is a variable amount of extinction across the OH bandpass, which means that as the airmass increases, the blueward emission lines are attenuated faster than the redward ones. The final series of tests evaluated how this variable extinction impacts the value of γ. The results of these tests indicate that, at five magnitudes of extinction, γ will vary by about 3%, primarily due to a weak 1-1 band emission line at the red end of the filter becoming more prominent. However, in practice, this 3% effect will be rapidly overwhelmed by the increasing uncertainties due to lower count levels at the higher extinction.

In summary, there are many factors that have the potential to alter the calibration coefficients: temperature variations, f-ratio, differences in the filter transmission curves, changes in the comet's heliocentric velocity and distance, and effects due to variable extinction across the bandpass. Fortunately, the majority of these influence the results at a level of a few percent or less in the HB filter system. In only two of these cases should there be concern for significant changes in the coefficients, and both of these are a concern only for the C_2 and C_3 filters. First, observers using telescopes with f-ratios less than $f/4$ should be aware that as the f-ratio gets smaller, the error in the calibrations gets larger. Second, the few recipients of filters that differ from the calibration filters might need to incorporate a correction to account for the different fraction of the emission spectrum that is being measured.

6. SUMMARY

This paper presents the final calibration results for the new HB narrowband comet filters. It introduces the new filters, describes the factors that were considered in the design and manufacturing process, and gives the specifications of the final product. Also discussed are the procedures used to calibrate the filters so that comet observations can be reduced to absolute fluxes. This process involved the establishment of a new magnitude system, the development of the data reduction procedures (including a new formalism that can account for any mutual contamination of filters), and the computation of reduction coefficients that are used in the final result. Tests indicate that the filters are very stable for use in all but the most extreme circumstances. In general, the only factor that will affect the calibrations at a level greater than a few percent is their use on telescope systems with f-ratios less than $f/3$.

During the establishment of the magnitude system, our analysis of the standard stars (both solar analogs and flux standards) showed that the spectrum of one star may be very different from another star in the near-UV, even though the two stars nominally have the same spectral type. On the other hand, at wavelengths above 4000 Å, stars of similar spectral type tend to be essentially the same. We also found that the Strömgren u–b color corresponds well to our near-UV results, so this parameter can be used as a preliminary diagnostic tool in the evaluation of other stars.

APPENDIX A

OH Extinction

A.1. Extinction Components in the OH Filter

The effects of atmospheric extinction in the OH filter, unlike the other filters, cannot be properly represented by a linear relation. This is due to the fact that the extinction has a strong wavelength dependence across the OH bandpass and due to a very small red leak (~0.03%) in the filter transmission at 3350 Å. Plotting the OH magnitudes versus the airmass at which they were obtained produces a curve, and forcing a linear fit to this curve will produce incorrect magnitudes when they are extrapolated to zero airmass. Furthermore, the extrapolated result will change if a different range of airmass is used, because a different section of the curve is being fit. Therefore, it is necessary to use models of atmospheric extinction to reproduce the curvature in the magnitude–airmass plot, so that a proper extrapolation to zero airmass can be done, regardless of the airmass range of the data.

There are three primary components to the extinction in the OH filter. The first, and simplest, component is Rayleigh scattering by molecules in the atmosphere, which is well-understood and can be accurately computed (e.g., Hayes and Latham 1975). It is a function of the elevation of the observing site (in which the atmosphere has a scale height of 7.5 km at 0°C) and varies as λ^{-4}. Rayleigh scattering contributes about 40–50% of the total extinction in the OH bandpass and has a slight slope which introduces a small amount of curvature to the magnitude–airmass relation.

The second extinction component is absorption by aerosols in the atmosphere. With a typical scale height of 1–2 km, this component is strongly affected by the elevation of the site, which means it can contribute 5–20% (or more) of the total extinction. This component varies as $\lambda^{-\alpha}$, where α can range from 0 to 1.5 (depending on the type of aerosols), with a typical value of 0.8; this means that the aerosol extinction is essentially flat across the OH filter bandpass.

The last and most complicated component is the absorption by ozone molecules in the stratosphere. Because the bulk of the ozone is located at an altitude of 15–30 km, the extinction is not dependent on the elevation of the observing site: however, the altitude does prompt the use of a local airmass, which will be defined later. This component, typically comprising 40–50% of the total extinction in the OH filter, is very sensitive to the amount of ozone above the observing site, defined in units of centimeters at standard temperature and pressure (a normal value falls in the range 0.2–0.3 cm). For wavelengths shortward of 3200 Å, the extinction due to ozone increases extremely rapidly, so that there is a steep slope even across the narrow OH bandpass. In addition, the ozone extinction is curved, not linear, across the bandpass. This steep slope, with an additional contribution from the curvature, is what produces the majority of the curvature in the magnitude–airmass relation. It should be noted that because this component drops so rapidly at longer wavelengths, it does not cause any problems in the other ten filters. (Although ozone contributes significantly for NH and at wavelengths between 5000 and 7000 Å, the extinction is flat enough that the effects of ozone are included in the linear extinction coefficient.)

As was suggested above, the elevation of the observing site is an important factor in the OH extinction problem. It affects the Rayleigh and aerosol components directly, and as will be seen later, this has an indirect effect on computing the ozone contribution. Thus, some of the equations given below include terms that account for the elevation, and these must be included to properly model the different components.

When the OH extinction from the extinction stars is solved for, and the results are applied to other objects, the easiest and most straightforward method is to address each of the three extinction components separately. This simplifies the problems involved with different elevation and airmass effects for the different components and makes it easier to solve for the curvature in the magnitude–airmass relation.

A.2. Airmass Calculations

Dealing with each of the three extinction components separately means that it is necessary to use different airmass computations, each of which is most suitable for the particular component to which it is applied. For the Rayleigh and aerosol components, Hardie's (1962) empirical formula is used:

$$X = \sec Z_{\text{app}} - 0.0018167(\sec Z_{\text{app}} - 1) - 0.002875(\sec Z_{\text{app}} - 1)^2 - 0.0008083(\sec Z_{\text{app}} - 1)^3. \quad (6)$$

In this equation, however, a Z_{app} that corrects for the elevation effects on the atmospheric refraction should be used,

$$Z_{\text{app}} = Z_{\text{true}} - \frac{60.4 \tan Z_{\text{true}} - 0.0668 \tan^3 Z_{\text{true}}}{3600} \exp(-h/8.0), \quad (7)$$

where h is the elevation of the observing site in kilometers and Z_{true}, in degrees, is computed from the object's right ascension and declination (e.g., Henden and Kaitchuck 1982).

For the ozone component, which does not extend all the way to the ground, a better airmass approximation uses a thin slab of atmosphere at a distance of 22 km above the ground. To account for the curvature of the Earth when looking downrange in this scenario, the slab is tilted so that it is parallel to the Earth's surface at the distance downrange where the line of sight intersects the slab. This defines the local zenith angle (e.g., Young 1974), from which the ozone airmass (X_{loc}) is found,

$$X_{\text{loc}} = \sec Z_{\text{loc}} \quad (8)$$

$$= \frac{R + H}{[(R + H)^2 - R^2 \sin^2 Z_{\text{true}}]^{1/2}}, \quad (9)$$

where $R = 6378$ km is the radius of the Earth and $H = 22$ km is the altitude of the slab.

A.3. OH Extinction Determination

This section describes how the separate components are determined from the extinction stars and then discusses how those results are applied to other objects. The procedures and equations presented here were developed to deal with the components separately and were tested on both B star and G star observations to ensure that they correctly reproduce the curvature in the magnitude–airmass relation. Because of differences in spectral distributions between B stars, G stars, and comets, some of the equations will have different coefficients for the different objects. These coefficients are listed in Table VIII.

Ultimately, the total extinction for each data point in the OH filter is determined from

$$m_0 = m - G_{R_{\text{OH}}} - E_{A_{\text{OH}}} X - G_{O_{\text{OH}}}, \quad (10)$$

where m is the object's measured magnitude, m_0 is the magnitude at zero airmass, $G_{R_{\text{OH}}}$ and $G_{O_{\text{OH}}}$ represent the total extinctions (in magnitudes) for the Rayleigh and ozone components, and $E_{A_{\text{OH}}}$ is the extinction coefficient (in magnitudes per airmass) for the aerosol component. Computation of the individual components is discussed next.

First, the total extinction from the Rayleigh component can be accurately computed using the airmass of the observation, X, and the elevation of the site, h, in kilometers,

$$G_{R_{\text{OH}}} = (b_1 X + b_2 X^2) \exp(-h/7.5), \quad (11)$$

where b_1 and b_2 are given in Table VIII and a scale height of 7.5 km (rather than 8) is used to account for the drop in scale height at higher elevations where OH is likely to be observed.

Because the amount of aerosols in the atmosphere changes from night to night (and even within a night), this component must be extracted from the extinction star observations. To avoid the problem of disentangling the aerosol and ozone contributions at OH, another filter, for which ozone extinction is negligible and the Rayleigh component is easily computed, is used to separate out the amount of aerosols. The BC filter is the best choice for this purpose. Not only is it the only filter that is common to all filter sets, but it gives a good signal-to-noise and ozone is negligible.

To determine the aerosol extinction, the linear extinction coefficient for the BC filter, E_{BC} (in magnitudes per airmass), is determined from the techniques described in Section 4.2; this coefficient represents the combined extinction from both the Rayleigh and the aerosol components. The Rayleigh component for the BC filter (0.2532 mag airmass^{-1} at sea level) is computed using

$$E_{R_{\text{BC}}} = 0.2532 \exp(-h/7.5) \quad (12)$$

which allows the aerosol component to be separated out for the BC filter:

$$E_{A_{\text{BC}}} = E_{\text{BC}} - E_{R_{\text{BC}}}. \quad (13)$$

The aerosol extinction varies with wavelength as $\lambda^{-\alpha}$, where α ranges from 0 to 1.5. Following Hayes and Latham (1975), 0.8 is adopted as a best average value, which is used to extrapolate the aerosol component from BC to OH:

$$E_{A_{\text{OH}}} = (3097/4453)^{-0.8} E_{A_{\text{BC}}}. \quad (14)$$

Using $\alpha = 0.8$ is a good approximation because the aerosol component comprises only a small portion of the total OH extinction; changes in α will propagate

TABLE VIII
Coefficients for OH Extinction

Coefficient	B star	G star	Comet[a] Pure OH	Comet[a] 25% continuum
		Rayleigh		
b_1	1.159	1.158	1.170	1.168
b_2	-4.433×10^{-4}	-5.359×10^{-4}	—	-1.918×10^{-4}
		Ozone		
c_{00}	1.323×10^{-2}	2.880×10^{-2}	—	-2.523×10^{-2}
c_{01}	-1.605×10^{-1}	-3.912×10^{-1}	—	4.382×10^{-1}
c_{02}	4.258×10^{-1}	1.597	—	−2.415
c_{03}	9.099×10^{-1}	-7.460×10^{-1}	—	4.993
c_{10}	-1.731×10^{-2}	-5.284×10^{-2}	-1.669×10^{-3}	4.276×10^{-2}
c_{11}	3.273	3.753	3.365	2.538
c_{12}	-2.815×10^{-1}	−2.632	-2.973×10^{-2}	4.109
c_{13}	−2.221	8.912×10^{-1}	—	−8.518
c_{20}	5.349×10^{-3}	2.634×10^{-2}	3.521×10^{-4}	-2.510×10^{-2}
c_{21}	-5.031×10^{-2}	-3.380×10^{-1}	-6.662×10^{-3}	4.148×10^{-1}
c_{22}	-4.182×10^{-1}	8.699×10^{-1}	-5.335×10^{-2}	−2.405
c_{23}	1.649	4.253×10^{-2}	—	4.666
c_{30}	2.810×10^{-4}	-3.141×10^{-3}	—	5.070×10^{-3}
c_{31}	-1.195×10^{-2}	3.359×10^{-2}	—	-8.168×10^{-2}
c_{32}	1.063×10^{-1}	-9.235×10^{-2}	—	4.272×10^{-1}
c_{33}	-3.877×10^{-1}	-1.677×10^{-1}	—	-8.618×10^{-1}

[a] Comet coefficients represent the extreme cases of pure OH emission and 25% underlying continuum.

through as a small variation on top of this already small fraction. Because the aerosol extinction is essentially flat, it has the same contribution for B stars, G stars, and comets.

Finally, the most complicated extinction component, ozone, must be determined. The slope and curvature of the ozone extinction preclude the use of a linear coefficient, and instead, a polynomial as a function of $X_{\rm loc}$ is used to solve for the total ozone extinction:

$$G_{O_{\rm OH}} = a_0 + a_1 X_{\rm loc} + a_2 X_{\rm loc}^2 + a_3 X_{\rm loc}^3. \quad (15)$$

To compound the issue, the coefficients in this polynomial are not constant; they are a function of the amount of ozone ($t_{\rm oz}$) that is present and are computed from the relations

$$a_0 = c_{00} + c_{01} t_{\rm oz} + c_{02} t_{\rm oz}^2 + c_{03} t_{\rm oz}^3 \quad (16)$$

$$a_1 = c_{10} + c_{11} t_{\rm oz} + c_{12} t_{\rm oz}^2 + c_{13} t_{\rm oz}^3 \quad (17)$$

$$a_2 = c_{20} + c_{21} t_{\rm oz} + c_{22} t_{\rm oz}^2 + c_{23} t_{\rm oz}^3 \quad (18)$$

$$a_3 = c_{30} + c_{31} t_{\rm oz} + c_{32} t_{\rm oz}^2 + c_{33} t_{\rm oz}^3, \quad (19)$$

where the c_{ij} coefficients are again listed in Table VIII. The OH extinction coefficients were produced by modeling the atmospheric extinction, as a function of airmass and ozone thickness, for each type of object (B star, G star, and comets) and then fitting polynomials to the results. The Rayleigh and aerosol models come from Hayes and Latham (1975) and the ozone extinction from McClatchy *et al.* (1978).

Thus, to determine the ozone extinction contribution, $t_{\rm oz}$ must be measured from a flux standard. This is done by first assuming $t_{\rm oz} = 0.150$ and extrapolating each measurement of an extinction star to above the atmosphere using Eqs. (10), (11), (14), and (15). The amount of scatter in the reduced magnitudes for all measurements of that star is then computed. Next, $t_{\rm oz}$ is increased in steps of 0.001 and the reduced magnitudes and their scatter are recomputed for each step. The value of $t_{\rm oz}$ that produces the minimum scatter represents the amount of ozone present during the observations. In other words, when $t_{\rm oz}$ produces the right amount of curvature in the magnitude–airmass relation, an extrapolation from each data point of an extinction star will result in the same magnitude at zero airmass. We tested this procedure on our standard star measurements and compared the computed $t_{\rm oz}$ to satellite measurements of the ozone (Earth Probe TOMS data) over Lowell Observatory. The results agree to within 4% for any given night and to within 2% when the satellite measurements indicate that the ozone thickness is stable from night to night for our observing location.

This entire process is repeated with each extinction star to obtain average values for the aerosol extinction and the ozone thickness. (Multiple star measurements also provide a means of tracking whether the aerosols and ozone were changing during the night.) The average values of $E_{A_{\rm OH}}$ and $t_{\rm oz}$ are then used to compute the OH extinction for any other objects observed during the night.

In summary, the extinction stars are used to compute two quantities relating to the OH filter: the extinction from aerosols and the amount of ozone in the atmosphere. The extinction for any other object's measurement is found by computing the Rayleigh component from Eq. (11), applying the aerosol coefficient at the proper airmass, and computing the ozone extinction from Eq. (15). This combination of the three components allows each data point to be extrapolated to a magnitude at zero airmass, by application of Eq. (10).

The reduction of comet data includes another step, however. Comet measurements consist of OH emission on top of continuum, and the values of c_{ij} will change, depending on the amount of continuum (which changes the flux distribution across the filter bandpass). To deal with this problem, two sets of coefficients were determined for the comet: one with pure OH emission and another in which 25% of the total flux is produced by continuum (practical extremes for most comets). The comet data are then reduced in two passes: In the first pass the coefficients for the pure OH case are used to determine the total amount of extinction. At the same time, the extinction for the 25% continuum case is also computed and saved. The pure OH extinction is then used to reduce the comet data to obtain the total band flux and the net OH flux, as described in Appendix D. During this process, the percentage of underlying continuum in the OH filter measurement is computed. Using this percentage, a second pass is made and the total extinction is recomputed by interpolating between the pure OH and the 25% continuum cases,

$$E_{\rm tot} = 4[(0.25 - P_c)E_{0\%} + P_c E_{25\%}], \quad (20)$$

where P_c is the percentage of underlying continuum in the OH filter, and $E_{0\%}$ and $E_{25\%}$ are the total extinctions computed with the pure OH and 25% continuum coefficients, respectively. $E_{\rm tot}$ is then used to re-reduce the comet OH data to their final results. With the new extinction value, the percentage of underlying continuum will also change slightly, but this will be less than a few percent, so further iterations on the total extinction are not necessary.

APPENDIX B

Computation of Standard Star Magnitudes

This appendix describes the procedures that were used to establish the standard star magnitude system for the HB filters. Before applying these procedures, all of the relevant nights of data were reduced, as described in the text, to obtain the instrumental magnitudes above the Earth's atmosphere. In addition, high airmass points, used to determine extinction coefficients, were removed so that only data obtained at an airmass of 2.1 or less were included in the final computation of the magnitudes.

As mentioned in the text, the HB magnitude system is based on semi-arbitrary values that are pre-assigned to the fundamental star (HD 191263). All other standard star magnitudes are computed relative to these values. The method for computing these magnitudes begins with the selection of a single night that will provide the initial data set. This first night is important because it serves as the basis for all other results; therefore, it must be of very high quality and have observations of as many stars as possible, including several measurements of the fundamental star. Next, the magnitude of HD 191263 is set to 6.19 in all filters (as discussed in Section 4.3). The measured values of HD 191263 are then used to compute the difference (Δm) between the pre-defined magnitude and the instrumental magnitude for each filter. Δm for each filter is simply the difference between the zero point of the instrumental and HB systems, and to first order, it is constant for all objects observed on a given night. Therefore, Δm is added to each of the other star measurements to convert their magnitudes to the HB systems. Where several observations exist, they are averaged, without weighting. This process produces a (very preliminary) HB magnitude system for those stars observed on the first night.

The second night must include several flux standards that were also observed on the first night, because the instrumental magnitudes are linked to the HB system through the stars whose magnitudes have already been determined. As on the first night, Δms are computed for each filter; however, in this case, all of the stars whose magnitudes have been computed are used in the average, rather than just the fundamental star; this keeps the fundamental star from being weighted more heavily than the other stars. Again, these average Δms are used to transform the data to HB magnitudes, which can then be incorporated into the HB magnitude averages. The rest of the nights are reduced in the same manner, recomputing the standard star magnitudes after each group of three or four nights has been reduced with the previous magnitudes. When all of the nights have been included, the first iteration is completed and a set of preliminary magnitudes has been defined. Because all available stars are used to compute the Δms at each step, the magnitude of HD 191263 may deviate from 6.19 in some (or all) filters. If this is the case, then the new averaged magnitudes of all the stars are arbitrarily shifted to bring the magnitudes of HD 191263 back to 6.19 to maintain the original definition of the standard star system.

The entire process, including the re-reduction of the raw data to instrumental magnitudes, can now be iterated to search for and remove any bad data points. When the standard star data were first reduced, the quality of the data could only be judged by looking at how well the extinction solution fit the extinction stars and how closely the solutions from different stars matched on that night.

This means that all of the data on a night were either included or rejected based on the extinction stars. With the preliminary magnitude system in place, all of the data can be re-reduced using the Δm for each individual data point as a means of identifying problem measurements in each night's measurements. In this manner, nights that are good overall can be used, while any poor quality data can be eliminated (e.g., it is easy to identify if and when clouds came in during a night by looking at the change in Δm). In addition, the magnitude system permits the use of a global solution for the extinction, so less-well-determined extinction coefficients can be adjusted to improve the overall fit to the data.

After the data have been re-reduced, the procedures for computing the magnitudes are repeated to get a second set of preliminary magnitudes. Further re-reductions and repetitions are done, until the magnitudes converge and all of the poor-quality data points have been eliminated. Note that each iteration of the magnitude calculations starts from scratch, with no information from the previous iteration other than the improved reduction of each night's data. The iteration process is primarily a means of cleaning up the data to eliminate problem points, but it also helps to keep the early nights from being weighted too heavily in the statistics (the re-reductions provide the feedback from the magnitudes determined in each pass). In general, the nights we used were of very high quality; however, the re-reduction process did help to identify two quasi-photometric nights that were ultimately removed from the averages. In addition, several nights started out photometric and then became cloudy, and the re-reduction helped to identify the point at which the data became questionable. Ultimately, the quality of our data was sufficient that only three iterations were necessary for the magnitudes to converge to final values.

As a consistency check, we also performed a separate, parallel computation, in which the colors were used to indirectly determine the magnitudes. In a procedure similar to that used to compute the magnitudes, the color for each measurement was computed from the instrumental magnitudes and an average Δ (Color) was determined for each filter. These were used to transform each measurement from instrumental colors to HB colors, which were then combined to get an overall average. Finally magnitudes were then obtained by adding the color for each filter to the BC magnitude for that star. The results of this computation were essentially identical to those obtained directly from the magnitudes, though the uncertainties differed slightly. The uncertainties in the color computations are actually smaller than in the magnitudes (e.g., any variation in conditions during a night affects all of the filters in the same manner); however, when the colors are converted back to a magnitude, the inclusion of the uncertainty in the BC magnitude raises the overall error to be equal to or slightly higher than those for the magnitudes determined directly.

APPENDIX C

Absolute Flux Calibration

Transforming relative magnitudes into absolute fluxes can be done using the standard equation

$$F_{\text{abs}} = F_0 10^{-0.4(m-0)}, \tag{21}$$

where F_0, the absolute flux of a 0 magnitude star, acts as the conversion coefficient. Thus, the absolute flux of a 0 magnitude star must be determined for each of the HB filters. To do this, we used HB standard stars that are listed in calibrated spectrophotometric catalogs (Breger 1976, Burnashev 1985, Hamuy *et al.* 1992, Kharitonov *et al.* 1988, Taylor 1984) and tied the system to an absolute flux based on the star Vega. The stars that we found in these catalogs, and were able to incorporate in to the computations, were HD 74280 (5 sources), HD 26912 (3), HD 164852 (2), HD 37112 (1), and HD 129956 (1). In addition, spectra of several of these stars from the otherwise unpublished collection of A'Hearn were used as a consistency check. Note that most catalogs provide only relative fluxes, or even magnitudes, at various wavelengths, so a roundabout computation must be used to obtain the absolute fluxes. Furthermore, some of the catalogs list only a few values at widely spaced wavelengths. Interpolating between these wavelengths is acceptable for most filters; however, in the region near the Balmer discontinuity, interpolating produces large errors. Thus, the flux at the CN filter was not computed from catalogs where this interpolation was required.

To couple the HB system to an absolute flux calibration, we adopted the Hayes and Latham (1975) standard, in which a V = 0 star has a flux at 5556 Å of $F_{0_V} = 3.52 \times 10^{-9}$ erg cm^{-2} s^{-1} Å^{-1}. This value is used, along with a standard star's V magnitude, to compute the flux of that star at 5556 Å. The absolute flux at the central wavelength of each HB filter is then found from the ratio of the flux at λ to the flux at 5556 Å as listed in the catalogs and scaling to the absolute 5556 Å flux determined previously. Finally, we used the absolute flux at a given filter, combined with the star's HB magnitude, to determine the absolute flux that would be produced in that filter by a 0 magnitude star. This was done for all of the filters in all of the available stars to get multiple estimates of the 0 magnitude flux, which were then combined to produce an average conversion coefficient for each filter. Although the process seems complicated, all of the steps listed above for a single star collapse to a relatively simple equation,

$$F_{0_{XX}} = F_{0_V} \frac{f_{XX}}{f_{5556}} 10^{0.4(m_{XX}-V)}, \tag{22}$$

where F_0 is the absolute flux of a 0 magnitude star in a given filter, f is the relative flux listed in the catalogs, m_{XX} is the star's HB magnitude in the XX filter, and V is its Johnson V magnitude. An analogous equation can be derived for catalogs that list magnitudes rather than fluxes.

APPENDIX D

General Reduction Procedures for Comet Observations

Because many observers are likely to use a subset of the 11 filters, this appendix outlines a set of reduction procedures that can be used in many situations, yet will still produce results that can be compared to those from observers with a different combination of filters. The following gives a list of steps in which the italicized text describes the task to be performed and the rest of the paragraph describes specifically how it is done. Many of the equations are generalized, with XX and YY representing the individual filter specifications. The relevant coefficients are listed in Tables VI and VII.

1. *Convert HB magnitudes to flux in arbitrary (linearized) units*. During the basic data reduction, the comet measurements are transformed into HB magnitudes above the Earth's atmosphere (m_{XX}) using the extinction coefficients and Δms determined from the standard stars (see standard star discussion for details). These magnitudes are then converted to linearized units (f_{XX}) using

$$f_{XX} = 10^{-0.4 m_{XX}} \tag{23}$$

which will be converted to an absolute flux in a later step. Note that f denotes the linearized units and f' (introduced below) denotes linearized units from which continuum and/or contamination have been removed. Similarly, F and F' denote, respectively, contaminated and decontaminated absolute fluxes.

2. *Decontaminate the continuum measurements and fill in for missing continuum values*. This is the most complicated of the steps, because of the process used for removal of contamination and how it is affected by missing filters. The continuum filters were designed to minimize the amount of contamination from undesired species: there is some C_2 contamination in the GC filter and some C_3 contamination in the UC filter, but otherwise the continuum bands are assumed to be clean. In actuality, each of the continuum filters is likely to contain some contamination from NH_2 or other short-lived species, but this is at a very low level (typically about 1%), and without measurements of these species, the contamination cannot be removed, in any case. Gas contamination of the continuum is removed using the measurement of the appropriate species. The amount of contamination is assumed to be a fixed fraction of the measured emission, so removing this flux from the continuum is, in principle, a simple matter. The catch is that, before the gas is removed from the continuum, the continuum must be removed from the gas measurement. This requires an iteration that reduces

the mutual contamination with each step. Tests performed with dusty, gassy, and average comets show that, in all cases, a maximum of three iterations is sufficient for convergence (to 1 part in 10^4).

In the case of missing continuum filter measurements, it is assumed that an observation was obtained with either the BC or the GC filter (or both), to provide a solid basis from which the continuum can be determined. If necessary, all other continuum fluxes can be determined from one of these filters, using solar colors. If more continuum filters have been measured, then dust colors (over and above the solar color) can be obtained and the underlying continuum flux can be more accurately removed from the gas measurements. Unfortunately, there is no way to account for missing gas filters, so if a C_2 or C_3 measurement is missing, the contamination to other filters cannot normally be removed, and it must be assumed that there is no contamination. If, however, it is a well-studied comet, it may be possible to use indirect methods to remove the contamination.

To start with, the BC and RC filters are both effectively clean, so the decontaminated flux can be considered to be the same as the contaminated value:

$$f'_{\rm BC} \equiv f_{\rm BC} \tag{24}$$

$$f'_{\rm RC} \equiv f_{\rm RC}. \tag{25}$$

If both the BC and the GC filters were measured, then the GC flux is decontaminated by iterating on the relation

$$f'_{\rm GC} = f_{\rm GC} - K_{\rm GC1} f_{\rm C_2} + K_{\rm GC3}(f'_{\rm BC})^{+0.1469}(f'_{\rm GC})^{+0.8531} \tag{26}$$

In this equation, the first term on the right side represents the measured GC flux, and the combined second and third terms represent the C_2 contamination: the C_2 measurement minus the underlying continuum (which is found by interpolating between the BC and the GC filters). $K_{\rm GC1}$ contains relevant information about the fraction of C_2 captured in the GC filter, along with the flux conversion from C_2 to GC. Similarly, $K_{\rm GC3}$ contains the same information as $K_{\rm GC1}$, but also accounts for the solar colors between the continuum filters and C_2. The exponents in the third term simply represent the interpolation between the BC and the GC filters. Initially, $f'_{\rm GC}$ on the right side is set equal to $f_{\rm GC}$, and the equation is iterated to solve for $f'_{\rm GC}$.

If the BC measurement is missing but GC was measured, then Eq. (26) cannot be solved. In this case, solar color is assumed between BC and GC and Eq. (26) reduces to

$$f'_{\rm GC} = f_{\rm GC} - \frac{K_{\rm GC1} f_{\rm C_2}}{1 - K_{\rm GC2}}, \tag{27}$$

which can be solved analytically to decontaminate the GC value. $K_{\rm GC2}$ contains information similar to $K_{\rm GC3}$, except that it applies the solar color to account for the fact that BC was not measured. After $f'_{\rm GC}$ has been determined, it is used to fill in the missing BC measurement (which will be used later):

$$f'_{\rm BC} = f'_{\rm GC} 10^{-0.4(m_{\odot\rm BC} - m_{\odot\rm GC})}. \tag{28}$$

In the same manner, a missing GC measurement can be filled in by extrapolating the solar color from the BC measurement;

$$f'_{\rm GC} = f'_{\rm BC} 10^{-0.4(m_{\odot\rm GC} - m_{\odot\rm BC})}, \tag{29}$$

which gives the decontaminated flux at the green continuum wavelength.

Finally, the UC filter is decontaminated using the relation (analogous to Eq. (26))

$$f'_{\rm UC} = f_{\rm UC} - K_{\rm UC1} f_{\rm C3} + K_{\rm UC3}(f'_{\rm BC})^{+0.6128}(f'_{\rm UC})^{+0.3872}, \tag{30}$$

which is, again, solved iteratively. Note that a BC value exists at this point (either measured or extrapolated from GC), so the alternate situation, corresponding to Eq. (27) in the GC case, is not relevant here. If the UC or RC measurement is missing, it can also be filled in using solar colors, but because these values are not used in the following, the equations are not given here.

3. *Compute the continuum colors*. We assume that the continuum colors (over and above the solar color) are linear with wavelength, when given in magnitudes. Thus, color terms can be defined for each wavelength segment between two filters: $R_{\rm UC-BC}$ is the continuum color from UC to BC; $R_{\rm BC-GC}$, from BC to GC; and $R_{\rm GC-RC}$, from GC to RC. All three are determined from the decontaminated filter measurements and are specified in magnitudes per 1000 Å:

$$R_{\rm UC-BC} = 0.998\left[2.5\log\frac{f'_{\rm BC}}{f'_{\rm UC}} - (m_{\odot\rm UC} - m_{\odot\rm BC})\right] \tag{31}$$

$$R_{\rm BC-GC} = 1.235\left[2.5\log\frac{f'_{\rm GC}}{f'_{\rm BC}} - (m_{\odot\rm BC} - m_{\odot\rm GC})\right] \tag{32}$$

$$R_{\rm GC-RC} = 0.535\left[2.5\log\frac{f'_{\rm RC}}{f'_{\rm GC}} - (m_{\odot\rm GC} - m_{\odot\rm RC})\right]. \tag{33}$$

If the BC or GC measurement is missing then $R_{\rm BC-GC}$ is set to zero to signify that only solar colors were used. As discussed in item 2, extrapolating the colors from UC or RC to fill in the BC to GC region can produce large errors, so it is safer to use the solar colors. On the other hand, if the UC or RC filter was not measured, then it is relatively safe to assume that the color in these regions is the same as between BC and GC ($R_{\rm UC-BC} = R_{\rm BC-GC}$ and $R_{\rm GC-RC} = R_{\rm BC-GC}$, respectively). This provides a better estimate of the continuum colors than simply using solar colors.

4. Compute the continuum underlying the gas and ion species. Once the continuum colors have been computed, then they are used to obtain the continuum flux underlying the gas and ion filters. If the BC flux is used as a basis, the color terms are used to extend to the other filters using the equations:

$$f'_{\rm OH_C} = f'_{\rm BC} 10^{-0.4(m_{\odot\rm OH} - m_{\odot\rm BC})} 10^{-0.5440 R_{\rm UC-BC}} \tag{34}$$

$$f'_{\rm NH_C} = f'_{\rm BC} 10^{-0.4(m_{\odot\rm NH} - m_{\odot\rm BC})} 10^{-0.4352 R_{\rm UC-BC}} \tag{35}$$

$$f'_{\rm CN_C} = f'_{\rm BC} 10^{-0.4(m_{\odot\rm CN} - m_{\odot\rm BC})} 10^{-0.2320 R_{\rm UC-BC}} \tag{36}$$

$$f'_{\rm C_{3C}} = f'_{\rm BC} 10^{-0.4(m_{\odot\rm C3} - m_{\odot\rm BC})} 10^{-0.1552 R_{\rm UC-BC}} \tag{37}$$

$$f'_{\rm CO^+_C} = f'_{\rm BC} 10^{-0.4(m_{\odot\rm CO^+} - m_{\odot\rm BC})} 10^{-0.0736 R_{\rm UC-BC}} \tag{38}$$

$$f'_{\rm C_{2C}} = f'_{\rm BC} 10^{-0.4(m_{\odot\rm C2} - m_{\odot\rm BC})} 10^{+0.2764 R_{\rm BC-GC}} \tag{39}$$

$$f'_{\rm H_2O^+_C} = f'_{\rm GC} 10^{-0.4(m_{\odot\rm H_2O^+} - m_{\odot\rm GC})} 10^{+0.7040 R_{\rm GC-RC}}. \tag{40}$$

Note that Eqs. (39) and (40) include coefficients different from the other equations, because they are not within the continuum region defined by the UC and BC filters.

5. Convert to absolute fluxes. At this point, all of the fluxes in arbitrary units are converted to absolute fluxes, so that the continuum can be properly subtracted and contamination removed from the gas measurements. Conversion of the decontaminated continuum measurements is done using

$$F'_{XX} = F_{0_{XX}} f'_{XX}, \tag{41}$$

where the XX denotes each of the continuum filters. The continuum underlying the emission bands is converted in the same manner,

$$F'_{YY_C} = F_{0_{YY}} f'_{YY_C}, \tag{42}$$

where the YY subscript denotes each of the gas bands and the C subscript indicates that this is the computed flux of the underlying continuum. The last

conversion is for the gas band measurements, which have not yet been decontaminated (hence, the lack of the prime symbol in the equation),

$$F_{YY} = F_{0_{YY}} f_{YY}. \tag{43}$$

Using the absolute continuum fluxes, $Af\rho$ values (in cm) can be computed for each of the continuum filters,

$$Af\rho = q_{XX} r^2 \Delta F'_{XX}/\theta, \tag{44}$$

where r and Δ are the heliocentric and geocentric distances to the comet (in AU), θ is the diameter of the aperture (in arcsec), and $q_{XX} = 2.4685 \times 10^{19}/F_{\odot XX}$ is a conversion factor specific to each filter: $q_{\rm UC} = 2.716 \times 10^{17}$, $q_{\rm BC} = 1.276 \times 10^{17}$, $q_{\rm GC} = 1.341 \times 10^{17}$, and $q_{\rm RC} = 1.975 \times 10^{17}$.

6. Remove continuum and contamination and convert to full band flux. Finally, the underlying continuum and gas contamination are removed from each emission species, and the measured flux is transformed, using the γ coefficients, to represent the entire band flux. Fortunately, there is no mutual contamination of two filters, so no iteration or simultaneous solutions are required. However, the order of solving the equations is important, because the filters contaminated by C_3 (NH, CN, CO^+) must be solved after the pure C_3 flux has been determined. The final gas fluxes are found from

$$F'_{\rm OH} = (\gamma_{\rm OH/OH})^{-1}\left[F_{\rm OH} - F'_{\rm OH_C}\right] \tag{45}$$

$$F'_{\rm C_3} = (\gamma_{\rm C_3/C_3})^{-1}\left[F_{\rm C_3} - F'_{\rm C_{3C}}\right] \tag{46}$$

$$F'_{\rm C_2} = (\gamma_{\rm C_2/C_2})^{-1}\left[F_{\rm C_2} - F'_{\rm C_{2C}}\right] \tag{47}$$

$$F'_{\rm NH} = (\gamma_{\rm NH/NH})^{-1}\left[F_{\rm NH} - F'_{\rm NH_C} - \gamma_{\rm NH/C_3} F'_{\rm C_3}\right] \tag{48}$$

$$F'_{\rm CN} = (\gamma_{\rm CN/CN})^{-1}\left[F_{\rm CN} - F'_{\rm CN_C} - \gamma_{\rm CN/C_3} F'_{\rm C_3}\right] \tag{49}$$

$$F'_{\rm CO^+} = (\gamma_{\rm CO^+/CO^+})^{-1}\left[F_{\rm CO^+} - F'_{\rm CO^+{}_C} - \gamma_{\rm CO^+/C_3} F'_{\rm C_3}\right] \tag{50}$$

$$F'_{\rm H_2O^+} = (\gamma_{\rm H_2O^+/H_2O^+})^{-1}\left[F_{\rm H_2O^+} - F'_{\rm H_2O^+{}_C}\right]. \tag{51}$$

The final results produced by the procedures outlined here are a measurement of the flux per unit wavelength at each continuum band and a measurement of the pure, full-band emission for each gas species.

ACKNOWLEDGMENTS

We thank the following for their contributions, without which this paper would not have been possible: Steve Larson for useful discussions on filter characteristics, Anita Cochran for providing the deVico and SW1 spectra for our calibration and testing, Roland Meier and Sang-Joon Kim for providing synthetic comet spectra, Wayne Osborn for discussions about the standard star magnitude computations, Jeff Hall and Wes Lockwood for helpful discussions about the solar analogs, Dennis Wellnitz and Alison Sherwin for measuring the transmission profiles of the filters and for contributing to the OH extinction calculations, Brian Skiff for advice in searching for the different types of standard stars, John Potter of Barr Associates for assistance in the filter design process, and Stephen White for information about the activity levels of the solar analogs. This research has made use of the Simbad database, operated at CDS, Strasbourg, France. This research has been supported by NASA Grants NAGW-5060, NAG5-6348, and NAG5-4146.

REFERENCES

A'Hearn, M. F. 1978. Synthetic spectra of C_2 in comets. *Astrophys. J.* **219**, 768–772.

A'Hearn, M. F. 1991. Photometry and polarimetry network. In *The Comet Halley Archive Summary Volume* (Z. Sekanina, Ed.), pp. 193–235. Jet Propulsion Laboratory, Pasadena.

A'Hearn, M. F., and J. J. Cowan 1975. Molecular production rates in Comet Kohoutek. *Astron. J.* **80**, 852–860.

A'Hearn, M. F., and R. L. Millis 1980. Abundance correlations among comets. *Astron. J.* **85**, 1528–1537.

A'Hearn, M. F., S. Hoban, P. V. Birch, C. Bowers, R. Martin, and D. A. Klinglesmith III 1986. Cyanogen jets in Comet Halley. *Nature* **324**, 649–651.

A'Hearn, M. F., R. L. Millis, and P. V. Birch 1979. Gas and dust in some recent periodic comets. *Astron. J.* **84**, 570–579.

A'Hearn, M. F., C. H. Thurber, and R. L. Millis 1977. Evaporation of ices from Comet West. *Astron. J.* **82**, 518–524.

Breger, M. 1976. Catalog of spectrophotometric scans of stars. *Astrophys. J. Supp.* **32**, 7–87.

Burnashev, V. I. 1985. Stellar spectrophotometric catalog. *Abastumanskaya Astrofiz. Obs. Bull.* **59**, 83.

Cayrel de Strobel, G. 1996. Stars resembling the Sun. *Astron. Astrophys. Rev.* **7**, 243–288.

Cochran, A. L., and W. D. Cochran 1991. The first detection of CN and the distribution of CO^+ gas in the coma of Comet P/Schwassmann-Wachmann 1. *Icarus* **90**, 172–175.

Cochran, A. L., W. D. Cochran, E. S. Barker, and A. D. Storrs 1991. The development of the CO^+ coma of Comet P/Schwassmann-Wachmann 1. *Icarus* **92**, 179–183.

Delgado, A. J., E. J. Alfar, and J. Cabrera-Caño 1997. CCD Strömgren photometry of young reddened stars. *Astron. J.* **113**, 713–721.

Farnham, T. L., and D. G. Schleicher 1997. Narrowband photometry of solar analogs in the near ultraviolet. In *Solar Analogs: Characteristics and Optimum Candidates* (J. C. Hall, Ed.), pp. 137–141. Lowell Observatory, Flagstaff.

Goy, G. 1980. Catalog General D'Etoiles de Type O. Donnes Spectroscopiques et Photometriques Bande Magnetique et Listage. *Astron. Astrophys. Supp.* **42**, 91–102.

Gunn, J. E., and L. L. Stryker 1983. Stellar spectrophotometric atlas, $3130 < \lambda < 10800$ Å. *Astrophys. J. Supp.* **52**, 121–153.

Hall, J. C., Ed. 1997. *Solar Analogs: Characteristics and Optimum Candidates*. Lowell Observatory, Flagstaff.

Hamuy, M., A. R. Walker, N. B. Suntzeff, P. Gigoux, S. R. Heathcote, and M. M. Phillips 1992. Southern spectrophotometric standards. I. *Publ. Astron. Soc. Pacific* **104**, 533–552.

Hardie, R. H. 1962. Photoelectric reductions. In *Astronomical Techniques* (W. A. Hiltner, Ed.), Chap. 8. Univ. of Chicago Press, Chicago.

Hayes, D. S., and D. W. Latham 1975. A rediscussion of the atmospheric extinction and the absolute spectral energy distribution of Vega. *Astrophys. J.* **197**, 593–601.

Henden, A. A., and R. H. Kaitchuck 1982. *Astronomical Photometry*, Willmann-Bell, Richmond.

Kharitonov, A. V., V. M. Tereshchenko, and L. N. Knyazeva 1988. *Spectrophotometric Catalog of Stars*, p. 484. *Alma-Ata, Nauka*, Moscow.

Kholopov, P. N., N. N. Samus, N. P. Kukarkina, G. I. Medvedena, and N. B. Perova 1981. 65th namelist of variable stars. *IAU Inf. Bull. Var. Stars* **1921**, 1–21.

Kim, S.-J., M. F. A'Hearn, and W. D. Cochran 1989. NH emissions in comets: Fluorescence vs collisions. *Icarus* **77**, 98–108.

Larson, S. M., Z. Sekanina, and J. Rahe 1991. Near-nucleus studies network. In *The Comet Halley Archive Summary Volume* (Z. Sekanina, Ed.), pp. 173–191. Jet Propulsion Laboratory, Pasadena.

McClatchy, R. A., R. W. Fenn, J. E. A. Selby, F. E. Volz, and J. S. Garing 1978. Optical properties of the atmosphere. In *Handbook of Optics* (W. G. Driscoll and W. Vaughan, Eds.), Section 14. McGraw-Hill, New York.

Meier, R., D. W. Wellnitz, S.-J. Kim, and M. F. A'Hearn 1998. The NH and CH bands of Comet C/1996 B2 (Hyakutake). *Icarus* **136**, 268–279.

O'Dell, C. R., and D. E. Osterbrock 1962. Emission band and continuum photometry of Comet Seki (1961f). *Astrophys. J.* **136**, 559–566.

Osborn, W. H., M. F. A'Hearn, U. Carsenty, R. L. Millis, D. G. Schleicher, P. V. Birch, H. Moreno, and A. Gutierrez-Moreno, 1990. Standard stars for photometry of comets. *Icarus* **88**, 228–245.

Schleicher, D. G. 1983. *The Fluorescence of Cometary OH and CN*, Ph.D. thesis, University of Maryland.

Schleicher, D. G., and M. F. A'Hearn 1988. The fluorescence of cometary OH. *Astrophys. J.* **331**, 1058–1077.

Schleicher, D. G., R. L. Millis, D. J. Osip, and P. V. Birch 1991. Comet Levy (1990c): Groundbased photometric results. *Icarus* **94**, 511–523.

Skiff, B. A. 1994. Photometry for stars in the field of V Bootis. *IAU Inf. Bull. Var. Stars* **4053**, 1–4.

Stone, R. P. S. 1977. Spectral energy distributions of standard stars of intermediate brightness. II. *Astrophys. J.* **218**, 767–769.

Swings, P. 1941. Complex structure of cometary bands tentatively ascribed to the contour of the solar spectrum. *Lick Obs. Bull. #508* **19**, 131–136.

Taylor, B. J. 1984. An augmented system of secondary standards for bright-star spectroscopy. *Astrophys. J. Supp.* **54**, 259–269.

Valk, J. H., C. R., O'Dell, A. L. Cochran, W. D. Cochran, C. B. Opal, and E. S. Barker 1992. Near-ultraviolet spectroscopy of Comet Austin (1989c1). *Astrophys. J.* **388**, 621–632.

Wehinger, P. A., S. Wyckoff, G. H. Herbig, G. Herzberg, and H. Lew 1974. Identification of H_2O^+ in the tail of Comet Kohoutek (1973f). *Astrophys. J.* **190**, L43–46.

Winkler, H. 1997. Red and infrared color of B stars and the reddening law of the galaxy. *Mon. Not. R. Astron. Soc.* **287**, 481–494.

Wolff, M. J., K. H. Nordsieck, and M. A. Nook 1996. A medium resolution search for polarimetric structure: Moderately reddened sightlines. *Astron. J.* **111**, 856–864.

Wyckoff, S., and P. A., Wehinger 1976. Molecular ions in comet tails. *Astrophys. J.* **204**, 604–615.

Young, A. T. 1974. Observational technique and data reduction. In *Methods of Experimental Physics, Vol. 12: Astrophysics, A* (N. Carleton, Ed.), Chap. 3. Academic Press, New York.